J. Fluid Mech. (2003), *vol.* 483, *pp.* 249–286.
DOI: 10.1017/S0022112003004221 Printed in the United Kingdom

Linear and nonlinear instabilities of a Blasius boundary layer perturbed by streamwise vortices. Part 2. Intermittent instability induced by long-wavelength Klebanoff modes

By XUESONG WU[1,2] AND MEELAN CHOUDHARI[3]

[1]Center for Turbulence Research, Stanford University, CA 94305, USA

[2]Department of Mathematics, Imperial College, 180 Queens Gate, London SW7 2BZ, UK

[3]Computational Modeling and Simulation Branch, NASA Langley Research Center, Hampton, VA 23681-2199, USA

(Received 28 January 2002 and in revised form 14 January 2003)

This paper presents theoretical results on the instability of a Blasius boundary layer perturbed by Klebanoff modes (i.e. the low-frequency streaks known to be induced by free-stream turbulence). Herein, the Klebanoff distortions are modelled as the signature of a three-dimensional convected gust that may be either isolated or periodic along the spanwise direction. Relatively weak Klebanoff fluctuations can produce $O(1)$ changes to the near-wall curvature of the base flow profile and, hence, fundamentally alter the nature of its instability characteristics. The perturbed flow is shown to support instabilities that are predominantly inviscid and have significantly larger growth rates and characteristic frequencies than the Tollmien–Schlichting (T–S) modes of an unperturbed Blasius flow. The spanwise mode shape of instabilities in the perturbed flow is determined by the Schrödinger equation, with a potential function that corresponds to the skin friction perturbation due to the Klebanoff distortion. The growth rates of these modes are determined by the near-wall torsion of the perturbed flow. The unsteadiness of the Klebanoff distortion is shown to be a crucial element in determining the overall instability characteristics.

A localized Klebanoff distortion supports both sinuous and varicose modes of instability, but the sinuous modes are generally more unstable than the varicose modes. Overall, the instability is intermittent in time and localized in space, being confined to certain parts of the modulation cycle and within a specific window(s) along the streamwise direction. In particular, the dominant sinuous modes appear only during the phase in which a low-speed streak dominates the Klebanoff distortion. A periodic distortion supports spatially quasi-periodic modes through a parametric resonance mechanism.

The theoretically predicted instability modes share some key features with the unstable disturbances measured in recent experiments, such as the relatively high frequencies, growth rates that depend on the level of free-stream turbulence, small rate of spreading in the lateral direction and, above all, their intermittency in space and time. Non-equilibrium critical-layer theory is used to track a localized sinuous mode through two distinct stages of nonlinear evolution, which eventually terminates in a singularity that indicates the onset of fully nonlinear yet primarily inviscid disturbance dynamics.

1. Introduction

It is known that low-frequency components of three-dimensional vortical disturbances in the free stream can be entrained into the boundary layer due to the non-parallel flow effect, producing significant distortion in the form of alternate thickening and thinning of the layer along the spanwise direction. This observation goes back to Dryden (1936) and Taylor (1939) who suggested that the entrained vortex motion, rather than the Tollmien–Schlichting (T–S) instability, was the leading cause of transition to turbulence. The dispute continued until the experiments of Schubauer & Skramstad (1947), which fully validated the work of Tollmien (1929) and Schlichting (1933) by suppressing the effects of free-stream turbulence. Since then, most studies have focused on transition in low-amplitude disturbance environments, for which the T–S modes provide the starting point for understanding the overall transition process.

Motivated by its relevance to turbomachinery, however, there has also been a considerable amount of work on transition at moderate to high levels of free-stream turbulence. This has renewed the interest in the findings of Dryden (1936) and Taylor (1939). Recent experimental studies (see e.g. Kendall 1985; Westin *et al.* 1994; Matsubara & Alfredsson 2001; and references therein) show that the boundary layer filters out the high-frequency components of free-stream turbulence, while amplifying the low-frequency parts of the signature. The distortion within the boundary layer is dominated by the streamwise velocity fluctuations, which are manifested in the form of longitudinal vortices or streaks. In recognition of the contribution by Klebanoff (1971), Kendall (1985) referred to these low-frequency streaks as the Klebanoff modes, and that name has been widely adopted in the literature since then. Since the Klebanoff modes do not mathematically correspond to eigensolutions of a linearized homogeneous boundary-value problem, in the present paper we shall refer to them as Klebanoff distortions or fluctuations in order to distinguish them from the instability modes that we shall discuss.

Given that Klebanoff fluctuations are of low frequency, one might be inclined to believe that an appropriate steady perturbation might capture the essential physics involved. Indeed, a steady perturbation in the oncoming flow can induce a boundary-layer distortion that is similar to the Klebanoff motions (Bradshaw 1965). Motivated by Bradshaw's observations, Crow (1966) calculated the resulting distortion using linearized boundary-layer equations and was able to describe the alternate thickening and thinning of the boundary layer near the leading edge as noted in the earlier experiments by Taylor (1939) and Bradshaw (1965). The boundary-layer response to small-amplitude unsteady vortical disturbances was calculated by Gulyaev *et al.* (1989) and Choudhari (1996) using the unsteady form of the linearized boundary-layer equations. They showed that the low-frequency disturbances induce a large streamwise velocity fluctuation in the boundary-layer region, which exhibits a significant growth in the downstream direction.

The boundary-layer approximation is valid sufficiently close to the leading edge, where the thickness of the boundary layer is smaller than the spanwise length scale of the perturbation. Due to a continued growth of the boundary-layer thickness (as well as of the perturbation amplitude), however, crossflow ellipticity (and disturbance nonlinearity) must become significant sufficiently far downstream of this region. The subsequent evolution of the boundary-layer signature of free-stream disturbances is described by the boundary-region equations (Goldstein & Leib 1993; Wundrow & Goldstein 2001; Leib, Wundrow & Goldstein 1999). Wundrow & Goldstein (2001) considered the generic case for purely steady perturbations, such that the nonlinearity

and crossflow ellipticity come into play simultaneously. In this case, the distorted flow differs from the original Blasius profile by $O(1)$ and, moreover, becomes inflectional in the main part of the boundary layer. It can therefore support a new and stronger class of inviscid Rayleigh instabilities, which may lead to the onset of turbulence via an alternative route to the T–S modes, namely bypass transition. Leib *et al.* (1999) used the linearized form of the unsteady boundary-region equations to describe the low-frequency Klebanoff fluctuation further downstream of the leading edge. By representing the broad-band free-stream turbulence as a superposition of Fourier modes, Leib *et al.* (1999) calculated the streamwise evolution of the root-mean-square of the fluctuations within the boundary layer, which compared favourably with the relevant experimental data. The boundary-layer response was found to be rather sensitive to the spectrum of the free-stream disturbance. Their findings underscore the importance of fully characterizing the free-stream environment; this has not been adequately done in most experiments.

As indicated above, experiments have provided fairly complete quantitative data about the characteristics of Klebanoff fluctuations themselves, and considerable theoretical progress has also been made in terms of characterizing/predicting them. However, the transition process in the presence of these fluctuations remains to be fully understood. In particular, it is not clear if the T–S waves continue to play an important part in transition or if it is initiated by some other instabilities, e.g. the instability of the streaks.

A number of direct laboratory investigations of the transition process in the presence of Klebanoff fluctuations have been made. At moderate levels of free-stream turbulence, Arnal & Juillen (1978) and Kendall (1990) have observed the intermittent appearance of wavepackets inside the boundary layer. While the exact origin of the wavepackets was unclear, they apparently resembled T–S waves. A series of landmark experiments conducted by Kendall has revealed some unusual characteristics of these wavepackets. First, they appear only when the free-stream turbulence level exceeds a threshold of about 0.1%. Second, the growth rates of these packets are considerably larger than those of the T–S waves, being also dependent on the turbulence level (Kendall 1991, 1998). Third, the frequencies of these waves are also higher than those of T–S instabilities. Finally, these packets are relatively confined in the spanwise direction, spreading rather slowly as they propagate downstream. There has been no physical explanation for the above features thus far, except for the conjecture by Goldstein & Wundrow (1998), that the intermittency of the wavepackets and the nonlinear dependence of their amplitude on the turbulence level could be attributed to random receptivity via non-parallelism of the mean flow (due to either a rapid boundary-layer growth near the leading edge and/or geometric perturbations in the region downstream). An alternative hypothesis (which does not preclude the scenario proposed by Goldstein & Wundrow) is suggested in the present study, which attempts to shed further light on some of the unusual characteristics of the high-frequency wavepackets noted above.

Rather than studying naturally occurring wavepackets, Watmuff (1997) used a harmonic point source to generate spanwise localized wavetrains in a controlled fashion. Even a weak Klebanoff perturbation was found to severely distort the wavetrain, such that a comparison with calculations that did not account for the Klebanoff distortions was almost meaningless. On the other hand, however, the artificially excited wavetrain did not exhibit the excess growth as observed by Kendall for the naturally occurring wavepackets. Watmuff attributed this difference to the fact that the Klebanoff fluctuations were relatively weak in his experiments.

Boiko *et al.* (1994) studied the development of an artificially excited planar T–S wave in a boundary layer subjected to 1.5% free-stream turbulence. As expected, the planar wave front was deformed by the Klebanoff fluctuations; however, the growth rate of the T–S wave was reduced (relative to that in an unperturbed Blasius flow), which suggests that the Klebanoff fluctuation now had a stabilizing effect on the unstable modes at higher frequencies. The ultimate breakdown of the laminar boundary layer was, however, still associated with the nonlinear development of the T–S wave. These observations present a rather paradoxical situation, since it is well known that higher-intensity free-stream turbulence generally hastens the laminar–turbulent transition. A similar problem was recently investigated by Watmuff (2000), albeit in a different experimental setting. He also observed the distortion of the wavefront, but found that the growth rate was hardly affected by the Klebanoff distortions. Nevertheless, transition in his experiments did occur slightly earlier than when the Klebanoff fluctuation was absent. Finally, Bakchinov *et al.* (1998) have investigated the interaction between a planar T–S wave of relatively high frequency and a localized disturbance introduced in the free-stream region. When generated separately, each of these disturbances was found to decay. But when introduced simultaneously, Bakchinov *et al.* observed enhanced amplification of broad-band low-frequency oblique waves, presumably due to a nonlinear interaction between the two artificially introduced disturbances. The nature of this interaction has not been explained as yet.

In addition to investigating the role of conventional T–S waves during transition under moderate levels of free-stream turbulence, it is also important to examine alternative instability mechanisms. Streak instability, in particular, has attracted much attention in recent years. Matsubara, Bakchinov & Alfredsson (2000) reported that streaks or Klebanoff modes are unstable, which can lead to a meandering and oscillation of the streaks and an eventual breakdown into turbulent spots. Unfortunately, the random nature of the streaks implies that a detailed quantitative study of their stability would be rather difficult. Therefore, some researchers have chosen to generate steady spanwise-dependent flow in a controlled manner, typically through surface suction/blowing or surface roughness. These artificially created distortions are akin to Klebanoff modes in some respects and, hence, these kinds of studies may shed useful light on the streak instability. For a survey of the main findings from these studies, the reader is referred to Part 1 of this paper (Wu & Luo 2003).

In an effort to understand streak breakdown, Andersson *et al.* (2001) modelled the streak structure as a steady, spanwise-periodic distortion to a Blasius boundary layer. An inviscid stability analysis based on Floquet theory suggested that the streaks become unstable only when the amplitude of the associated streamwise velocity perturbation exceeds approximately 26% of the free-stream velocity. This estimate is perhaps too high to be representative of typical Klebanoff distortions in natural disturbance environments. Based on the present work, it appears that a partial explanation for this discrepancy may well be related to the unsteadiness of the Klebanoff distortion, which (in spite of the low frequencies of the distortion) is found to exert a significant effect on the high-frequency secondary instabilities (see § 2.2). For distortion induced by a steady free-stream disturbance, Goldstein & Wundrow (1998) and Wundrow & Goldstein (2001) found that nonlinear effects cause the streamwise velocity to become large in localized regions of flow even when the root-mean-square (RMS) value of the distortion is relatively small, suggesting that a localized instability may occur first.

A direct numerical simulation of the transition initiated by high levels of free-stream turbulence was first performed by Rai & Moin (1993). Their simulations involved three sequential streamwise domains in order to cope with the different resolution requirements associated with the three dominant physical processes relevant to this problem, namely (*a*) interaction of free-stream turbulence with the leading edge, (*b*) subsequent development of the disturbance within the boundary layer plus the early transition stage, and (*c*) the late stages of transition plus the fully turbulent state. This treatment allowed a realistic description of the practical situation while avoiding the excessive grid count that would otherwise have been required.

Jacobs & Durbin (2001) carried out a direct numerical simulation of the bypass transition caused by strong free-stream disturbances, which were represented by a superposition of modes from the continuous spectrum of the Orr–Sommerfeld equation. Unlike Rai & Moin (1993), the perturbation was imposed at some large distance downstream from the leading edge. Due to the reduced size of the simulation domain and the increased computational power available, Jacobs & Durbin were able to perform the simulation on a finer mesh than was available to Rai & Moin (1993). It was found that the boundary-layer response was indeed dominated by streamwise streaks. However, these streaks appeared to be fairly stable and it was only after they had lifted up to the outer part of the boundary layer to form a 'backward jet' that the breakdown to turbulent spots occurred. Their simulation also revealed that the breakdown was local (as conjectured theoretically by Goldstein & Wundrow 1998 and Wundrow & Goldstein 2001), being determined by a combination of the strength and the length scale of the local distortion; the collective instability of the Floquet type was not observed.

In this paper, we investigate the instability of a Blasius boundary layer perturbed by Klebanoff distortions. Our main interest will be in small-amplitude distortions, partly because they allow the phenomenon to be studied on an analytical basis but also because the amplitude levels measured in most experiments do not exceed 10–15% of the free-stream velocity. Of course, a low level of disturbance in terms of RMS does not necessarily guarantee its linearity, as indicated by the work of Goldstein & Wundrow (1998) for the steady distortion mentioned earlier. However, we will show that certain unsteady distortions can alter the flow instability before reaching the nonlinear stage. One significant assumption underlying the present work involves the spanwise length scale of the Klebanoff distortion, which is assumed to be larger than the boundary-layer thickness. As in Part 1, we address two main issues: (*a*) how the Tollmien–Schlichting instability, which operates in the absence of any distortion, is modified by a weak Klebanoff fluctuation, and (*b*) whether a weak distortion can induce an inviscid instability which is absent from the unperturbed boundary layer. An asymptotic approach based on the high-Reynolds-number assumption is employed to describe both the Klebanoff fluctuation and the instability of the perturbed flow in a systematic and consistent manner.

In § 2, we formulate the problem in an asymptotic framework. A three-dimensional vortical disturbance is prescribed in the oncoming flow. The spanwise distribution of the perturbation is allowed to be either localized or periodic. The relevant inviscid solution, valid outside of the boundary layer, is obtained first. For the scalings adopted in this paper, the boundary-layer signature of this inviscid perturbation, i.e. the Klebanoff distortion, is governed by the linearized unsteady boundary-layer equations. In § 2.2, we present the details of the scaling arguments which determine both the characteristic wavelength of the instability modes as well as the required magnitude of the Klebanoff distortion. Depending on the relative values of the streamwise and

spanwise length scale of the instability, two distinct types of instability modes may be considered. The first class of modes corresponds to the fully three-dimensional (i.e. oblique) modes that were identified by Goldstein & Wundrow (1995) in the context of purely stationary distortions to a Blasius flow. The other set of modes is primarily two-dimensional, i.e. it has significantly shorter wavelengths in the streamwise direction than the spanwise length scale involved. The latter scale is, of course, the same as that of the distortion for both classes of modes. The Goldstein–Wundrow (G–W) modes are based on a parametric resonance mechanism, and therefore exist only for global distortions that are periodic in the spanwise direction.

The linear instability of the modified flow is analysed in § 3. Due to our interest in high-frequency wavepackets that are localized along the spanwise direction, the case of localized distortions (and, therefore, the second class of instabilities mentioned above) is emphasized in this paper. We show that the spanwise mode shape of the instability is governed by a Schrödinger equation, which describes the interaction between the instability mode and the Klebanoff distortion within the bulk of the boundary layer. The potential function in this Schrödinger equation is proportional to the local wall-shear perturbation induced by the the Klebanoff distortion. The growth rate of the instability mode is determined at a higher order in the asymptotic analysis, by the curvature of the distorted flow at the critical level of the instability mode. For a localized distortion, solutions representing sinuous and varicose modes are presented, and their relative importance is assessed. Further calculations are carried out for a spanwise localized Klebanoff fluctuation to demonstrate the intermittent and local nature of the instability.

The nonlinear development of a sinuous instability mode through a sequence of distinct asymptotic sub-regimes is considered in § 4. In § 5, we discuss how the preceding analysis can be applied to the case of spanwise-periodic Klebanoff distortions. The main findings of this work and their physical implications are summarized in § 6.

2. Formulation

Consider the two-dimensional incompressible boundary layer due to a uniform flow with velocity U_∞ past a semi-infinite flat plate. Superimposed on the incoming stream is a small-amplitude three-dimensional vortical disturbance (i.e. a 'gust') that is assumed to be advected at the free-stream speed. For simplicity, we also assume that the free-stream disturbance is harmonic in time, with a frequency of $k_1 U_\infty/\Lambda$ where k_1 denotes the non-dimensional frequency parameter and Λ represents the dimensional length scale of the gust in the spanwise direction.

The flow is described in the Cartesian coordinate system (x, y, Z), which has its origin at the plate leading edge. Here, x, y and Z denote the streamwise, normal, and spanwise coordinates non-dimensionalized with respect to Λ. The time variable t is normalized by Λ/U_∞ and the velocity components (u, v, w) and pressure p are normalized by U_∞ and ρU_∞^2, respectively, where ρ denotes the fluid density. The Reynolds number

$$R_\Lambda \equiv U_\infty \Lambda/\nu$$

is assumed to be a large parameter throughout this analysis (i.e. $R_\Lambda \gg 1$).

The streamwise and normal velocity components of the Blasius flow are given by

$$(U_B, V_B) = \left\{F'(\eta), (2xR_\Lambda)^{-1/2}(\eta F' - F)\right\},$$

where F satisfies the Blasius equation

$$F''' + FF'' = 0, \quad F(0) = F'(0) = 0, \quad F'(\infty) \to 1, \quad \text{with} \quad \eta = R_A^{1/2} \frac{y}{\sqrt{2x}}. \tag{2.1}$$

2.1. *Flow distortion induced by Klebanoff modes*

The boundary-layer response to a three-dimensional convected gust was analysed by Gulyaev *et al.* (1989), Choudhari (1996) and Leib *et al.* (1999). Similarly to their work, the velocity field of the disturbance superimposed on the oncoming flow has the form

$$\boldsymbol{u}_\infty = \epsilon_D(\hat{u}_\infty B'(Z), \hat{v}_\infty B'(Z), \hat{w}_\infty B(Z))\, \mathrm{e}^{\mathrm{i}k_1(x-t)+\mathrm{i}k_2 y}, \tag{2.2}$$

where ϵ_D represents the gust amplitude ($\epsilon_D \ll 1$), and k_1 and k_2 denote the streamwise and transverse wavenumbers, respectively. As shown in the above studies, the amplification of the gust signature within the boundary layer is directly proportional to the ratio of the spanwise and streamwise wavenumbers, respectively. Accordingly, we assume that $k_1 \ll 1$, $k_2 = O(1)$. For the most part, our interest will be confined to the range of streamwise locations that corresponds to

$$x \ll R_A, \tag{2.3}$$

so that the spanwise length scale of the disturbance is significantly greater than the local thickness of the boundary layer, and

$$x \ll \epsilon_D^{-1}, \tag{2.4}$$

which allows the effects of disturbance nonlinearity to be suppressed as the gust is advected with the free stream (Leib *et al.* 1999). We observe that the measured properties of Klebanoff modes are closely tied to the wavenumber–frequency spectrum of turbulence in the upstream flow and, therefore, will vary from facility to facility as well as between wind tunnels and the flight environment. Therefore, the accuracy of the 'long spanwise-wavelength' assumption will accordingly vary from one disturbance environment to another. For example, as pointed out by Leib *et al.* (1999), the measured length scale of Klebanoff fluctuations was nearly five times larger than the boundary-layer thickness in the original experiments of Klebanoff (1971); however, the scale was closer to the boundary-layer thickness in the experiments by Kendall (1985) and Westin *et al.* (1994). In the present context, of course, the assumptions (2.3) and (2.4) have been motivated primarily by the resulting simplicity of the analysis.

Note that we have allowed for a general spanwise dependence of the gust via the arbitrary function $B(Z)$. This generalization was prompted by the fact that, in practice, the free-stream disturbances are stochastic in nature, having a finite correlation length along the spanwise direction. Any given realization may, therefore, resemble a finite-extent perturbation rather than a spanwise-periodic one. In a broad sense, consideration of an isolated distortion is also motivated by the finding of Goldstein & Wundrow (1998) and Wundrow & Goldstein (2001) that a periodic distortion, under nonlinear effects, tends to concentrate in localized regions along the spanwise direction. A similarly general dependence of the free-stream disturbance, either on x (or, equivalently, on t due to the convective phase) and/or on y, may also be allowed for in this framework via a Fourier superposition. However, for simplicity, we will proceed on the basis of the harmonic assumption (2.2) and, later, indicate how the final results may be generalized to an arbitrary form of convected free-stream vorticity.

The inviscid solution (valid outside of the main boundary layer) for $k_1 x = O(1)$ can be written as (Leib *et al.* 1999)

$$\boldsymbol{u}_D = \boldsymbol{u}_\infty + \epsilon_D \nabla\phi, \tag{2.5}$$

where ϕ denotes the velocity potential and, to the required order, it satisfies the Laplace equation

$$\nabla^2\phi = 0. \tag{2.6}$$

The boundary conditions are given by

$$\left.\begin{array}{l} \nabla\phi \to 0 \quad \text{as} \quad y \to \infty, \\ \phi(x,0) = 0 \quad (x<0), \quad \phi_y(x,0) = -\hat{v}_\infty B'(Z)\,\mathrm{e}^{\mathrm{i}k_1(x-t)} \qquad (x>0). \end{array}\right\} \tag{2.7}$$

The full solution to the boundary-value problem (2.6)–(2.7) can be found by the standard Wiener–Hopf technique. However, for the purpose of stability analysis, we confine ourselves to the region $x \gg 1$, such that $k_1 x = O(1)$ while (2.3) is still satisfied. The inviscid solution under these conditions can be obtained by neglecting the x-derivative term in (2.6) and solving the resultant two-dimensional Laplace equation in the half-space $y > 0$. This yields the following solution for the slip velocity components in the streamwise and spanwise directions:

$$u_s \approx \hat{u}_\infty, \quad w_s \approx \hat{v}_\infty \frac{\partial}{\partial Z}\int_{-\infty}^{\infty} \frac{B(\zeta)}{\zeta - Z}\,\mathrm{d}\zeta. \tag{2.8}$$

The signature of the above inviscid solution within the boundary layer corresponds to a small perturbation to the Blasius flow and, to the leading order of approximation, is given by

$$\boldsymbol{u}_D = \epsilon_D \left[\tilde{U}, \left(\frac{2\bar{x}k_1}{R_\Lambda}\right)^{1/2}\tilde{V}, \tilde{W}\right]\mathrm{e}^{-\mathrm{i}\bar{t}} + \text{c.c.} + \ldots, \tag{2.9}$$

where we have put

$$\bar{x} = k_1 x, \quad \bar{t} = k_1 t.$$

Irrespective of the value of the transverse wavenumber k_2 or the spanwise distribution $B(Z)$, the solution for the boundary-layer distortion can be split into a sum of two parts:

$$(\tilde{U}, \tilde{V}, \tilde{W}) = \left[-\frac{w_s'(Z)}{k_1}\bar{U}, -\frac{w_s'(Z)}{k_1}\bar{V}, w_s(Z)\bar{W}\right] + u_s[\bar{U}_1, \bar{V}_1, 0] + \ldots. \tag{2.10}$$

Since $k_1 \ll 1$ for the low-frequency Klebanoff fluctuation, the second part is asymptotically smaller than the first and, therefore, does not influence the stability of the distorted flow to the leading order. Accordingly, only the first part of the Klebanoff distortion in (2.10) needs to be considered in the present work. Equation (2.10) also shows that the streamwise velocity perturbation within the boundary layer is much larger in amplitude than the free-stream disturbance. The functions $(\bar{U}, \bar{V}, \bar{W})$ are governed by the linearized unsteady boundary-layer equations (Leib *et al.* 1999)

$$\frac{\partial\bar{U}}{\partial\bar{x}} - \frac{\eta}{2\bar{x}}\frac{\partial\bar{U}}{\partial\eta} + \frac{\partial\bar{V}}{\partial\eta} + \bar{W} = 0, \tag{2.11}$$

$$-\mathrm{i}\bar{U} + F'\frac{\partial\bar{U}}{\partial\bar{x}} - \frac{F}{2\bar{x}}\frac{\partial\bar{U}}{\partial\eta} - \frac{\eta F''}{2\bar{x}}\bar{U} + F''\bar{V} = \frac{1}{2\bar{x}}\frac{\partial^2\bar{U}}{\partial\eta^2}, \tag{2.12}$$

$$-\mathrm{i}\bar{W} + F'\frac{\partial\bar{W}}{\partial\bar{x}} - \frac{F}{2\bar{x}}\frac{\partial\bar{W}}{\partial\eta} = \frac{1}{2\bar{x}}\frac{\partial^2\bar{W}}{\partial\eta^2}, \tag{2.13}$$

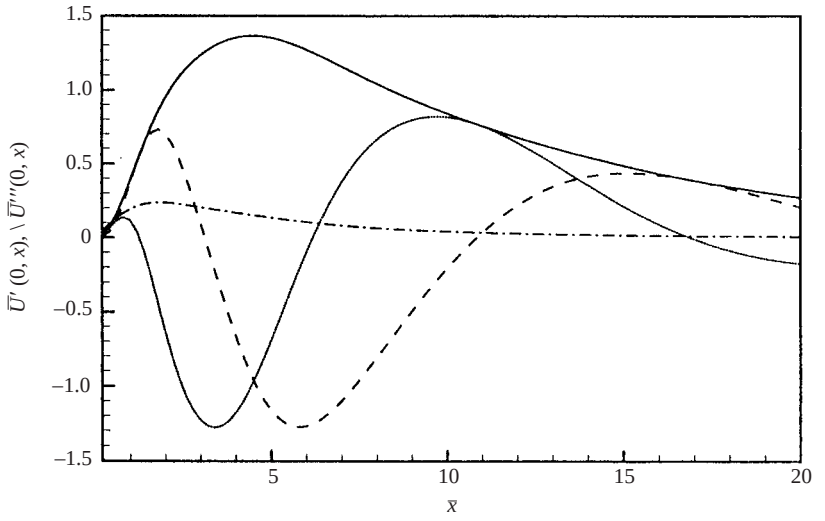

FIGURE 1. Variation of $U'''(0,\bar{x})$ (—, real part; - - - -, imaginary part) and $|U'(0,\bar{x})|$ (— · — · —) with $\bar{x}$.

where η is defined by (2.1). The appropriate boundary conditions are

$$\left.\begin{aligned} &\bar{U} = \bar{V} = \bar{W} = 0 \quad \text{at} \quad \eta = 0, \\ &\bar{U} \to 0, \quad \bar{W} \to \mathrm{e}^{\mathrm{i}\bar{x}} \quad \text{as} \quad \eta \to \infty. \end{aligned}\right\} \tag{2.14}$$

In the upstream limit ($\bar{x} \to 0$), the flow becomes quasi-steady and its solution matches that obtained by Crow (1966),

$$\bar{U} \to \tfrac{1}{2}\bar{x}\eta F'', \quad \bar{V} \to \tfrac{1}{4}(\eta^2 F'' - 3\eta F' - F), \quad \bar{W} \to F'. \tag{2.15}$$

On the other hand, as $\bar{x} \to \infty$, the perturbations move away from the wall and towards the edge of the mean boundary layer (Choudhari 1996; Leib *et al.* 1999). Because the maximum distortion to the boundary-layer flow is confined to the region $\bar{x} = O(1)$, this is the region of interest from the standpoint of investigating potentially radical changes to the linear instability of the flow.

We will show in § 3 that the complete profiles of the Klebanoff distortion are not required to determine the leading-order instability characteristics of the perturbed flow; instead, the characteristics are completely determined by local values of the slope $\bar{U}'(0,\bar{x})$ and the torsion $\bar{U}'''(0,\bar{x})$ of the streamwise velocity fluctuation near the surface. In fact, the wall torsion itself is related to the wall-shear perturbation by the simple relation

$$\bar{U}'''(0,\bar{x}) = -2\mathrm{i}\bar{x}\bar{U}'(0,\bar{x}), \tag{2.16}$$

which follows from a differentiation of (2.12) with respect to η and setting $\eta = 0$. The importance of the near-wall features of the gust signature is easily understood by recalling that the viscous instability modes of the unperturbed Blasius flow are controlled by the mean value of the skin friction parameter and, as noted by Goldstein & Wundrow (1998), any inflectional behaviour of the perturbed base flow is also confined to a narrow vicinity of the surface (since the amplitude of the Klebanoff distortion is assumed to be small in comparison with the free-stream speed). The streamwise variation in the amplitudes of the wall-shear and wall-torsion fluctuations due to the gust is displayed in figure 1, which underscores the previously made observation that the region $\bar{x} = O(1)$ accounts for the range of locations (or,

equivalently, the range of frequencies at a given streamwise location) wherein the boundary-layer flow is distorted the most.

2.2. *Scaling arguments*

As discussed in § 2.1, the Klebanoff distortion in the boundary layer is concentrated in the streamwise region where $\bar{x} = O(1)$, i.e. at a distance of $l^* = O(k_1^{-1}\Lambda)$ downstream from the leading edge. Accordingly, we introduce the Reynolds number based on l^*:

$$R = \frac{U_\infty l^*}{\nu} = R_\Lambda\left(\frac{l^*}{\Lambda}\right). \tag{2.17}$$

The base flow which has been distorted by this low-frequency fluctuation is inhomogeneous in both space and time. Although no comprehensive theory exists to describe the complete instability characteristics of such flows, we will exploit the weakness of the inhomogeneity to identify some of the interesting features of this instability.

Similarly to the case of purely steady distortions due to streamwise vortices (Goldstein & Wundrow 1995; Part 1), the spanwise velocity perturbation induced by the Klebanoff fluctuation is small compared with the corresponding perturbation in the streamwise velocity. Therefore, to the leading order of approximation, the modified base flow corresponds to a unidirectional shear flow, with the primary shear being along the wall-normal direction and a secondary shear along the spanwise coordinate. Such flows can support viscous–inviscid interactive instabilities with $O(R^{1/4}U_\infty/l^*)$ frequencies, which are governed by the triple-deck structure (Smith 1979). However, it is easily verified that the amplitude of the Klebanoff distortion must be comparable to the free-stream speed in order to produce an $O(1)$ change in the growth rates of these instability modes. In contrast, even relatively weak Klebanoff distortions can have a significant effect on the instability modes at higher frequencies (compared with those of the viscous–inviscid interactive modes), whose growth characteristics are controlled by the curvature of the perturbed flow in the vicinity of the wall. An important observation in this context is that, for the low-frequency (but unsteady) distortion,

$$\bar{U}'' \sim \eta \quad \text{as} \quad \eta \to 0. \tag{2.18}$$

Therefore, in a thin region near the surface, the Klebanoff fluctuation at suitable values of k_1 and ϵ_D may alter the curvature of the unperturbed Blasius profile by $O(1)$, while the perturbation to the streamwise velocity itself remains small compared with the free-stream speed. This, in turn, can lead to fundamental changes in the nature of instability in the distorted flow, by allowing inviscid instability modes to exist in addition to the primarily viscous T–S modes supported by the Blasius flow. The above scenario is rather different from the case where the distortion is induced by a completely steady free-stream disturbance†, for which $\bar{U}'' \sim \eta^2$ as $\eta \to 0$ and, therefore, no new instability can emerge until the distortion amplitude becomes $O(1)$. Thus, there exists a crucial difference between steady and unsteady distortions, even if the frequency of the distortion is significantly smaller than that of the instability modes.

The curvature of the distorted streamwise profile becomes comparable with that of the Blasius profile itself within a thin region near the wall. The $O(\hat{\sigma})$ thickness

† Here the distortion is caused by perturbations outside the boundary layer. The steady distortion considered in Part 1 is generated by perturbations within the boundary layer, and thus has a rather different vertical structure.

of this region (relative to the $O(R^{-1/2}l^*)$ thickness of the mean boundary layer) is determined by the balance

$$\epsilon_D \hat{\sigma}(l^*/\Lambda) \sim \hat{\sigma}^2. \tag{2.19}$$

Given the possible occurrence of an inflection point at $O(\hat{\sigma})$ distances from the surface, it follows from the classical Rayleigh scalings that the most unstable inviscid modes will have $O(\hat{\sigma}U_\infty)$ phase speeds and $O(\hat{\sigma}^{-1}R^{-1/2}l^*)$ wavelengths along the streamwise direction. Furthermore, consistent with our focus on local distortions, we seek instability modes with streamwise wavelengths shorter than the spanwise length scale of Λ.

The spanwise mode shape of the above instabilities (and their growth rate) is determined by the spanwise distribution of the Klebanoff distortion at the location of interest, similar to the instability modes considered in Part 1 (which involved purely stationary distortions). A crucial difference from Part 1 is that the curvature of the Klebanoff distortion is smaller by a factor $\hat{\sigma}$ in the wall layer than in the main part of the boundary layer. Unlike in Part 1, therefore, the instability characteristics of the perturbed flow are not solely controlled by the distortion in the wall region. The $O(\hat{\sigma})$ distortion in the bulk of the boundary layer also affects the instability wave, by inducing a comparable correction to the wavenumber and the phase speed. The distortion is a function of Z, and so must be the spanwise shape of the instability mode; however, the correction to the wavenumber must be Z-independent. Both the mode shape and the wavenumber correction must be determined through an appropriate eigenvalue problem. A careful consideration of the balances in the main deck shows that for a proper eigenvalue problem to be formulated at $O(\hat{\sigma})$, we require

$$\hat{\sigma}^{3/2} \sim \frac{R^{-1/2}l^*}{\Lambda}. \tag{2.20}$$

The exact reason for choosing the above scaling will become clear in the next section.

It is easy to deduce from (2.17), (2.19) and (2.20) that the width of the wall layer $\hat{\sigma}$ is related to the Reynolds number R_Λ and the frequency k_1 of the Klebanoff fluctuation via

$$\hat{\sigma} \sim (R_\Lambda/k_1)^{-1/3}, \tag{2.21}$$

and that the required amplitude of the free-stream disturbance is

$$\epsilon_D \sim k_1\hat{\sigma} \sim R_\Lambda^{-1/3}k_1^{2/3}. \tag{2.22}$$

We thus set

$$\epsilon_D = R_\Lambda^{-1/3}k_1^{2/3}B_0,$$

so that $B_0 = O(1)$ denotes the scaled amplitude of the distortion.

It can be shown that for the Klebanoff distortion to induce an $O(1)$ (or larger) change in the viscous growth rate of the instability modes of interest (relative to that in an unperturbed Blasius flow), we must have $\hat{\sigma} \gg R^{-1/20}$. On the other hand, recall that the foregoing analysis was based on the assumption that $\hat{\sigma} \ll 1$. These considerations impose the following restriction on the ratio k_1 of the spanwise and streamwise length scales of the Klebanoff distortion:

$$R_\Lambda^{-1} \ll k_1 \ll R_\Lambda^{-17/23}, \tag{2.23}$$

or, equivalently, on the range of streamwise locations where the analysis in §§3–4 is formally valid:

$$R_\Lambda^{17/23} \ll \frac{l^*}{\Lambda} \ll R_\Lambda. \tag{2.24}$$

Correspondingly, the amplitude of the free-stream disturbance can be anywhere within the range

$$R_\Lambda^{-1} \ll \epsilon_D \leqslant R_\Lambda^{-19/23}. \tag{2.25}$$

While the Klebanoff distortion modulates the Blasius flow on the slow variables $\bar{x}$ and $\bar{t} = k_1 t$, the instability wave oscillates on the much faster variables $\hat{\sigma} R^{1/2}\bar{x}$ and $\hat{\sigma}^2 R^{1/2}\bar{t}$. We thus introduce

$$\zeta = \hat{\sigma} R^{1/2}(\alpha\bar{x} - \hat{\sigma}\omega\bar{t}\,), \tag{2.26}$$

to describe the oscillation of the carrier wave, where the scaled wavenumber and frequency α and ω are both $O(1)$. In a flow that is slowly varying in the streamwise direction, it is natural to consider spatial instability. Since the present flow modulates in both time and space, one may equally argue for a temporal instability. It turns out that the spatial (temporal) growth rate $-\alpha_i$ (ω_i) of the instability mode is smaller than the wavenumber (frequency) so that $-\alpha_i$ and ω_i are linked by Gaster's (1962) relation, $-\alpha_i = \omega_i / c_g$, where the group velocity c_g is twice the phase speed c. In the following, a spatial instability problem will be formulated, i.e. ω is taken to be real and α expands as

$$\alpha = \alpha_0 + \hat{\sigma}\alpha_1 + \hat{\sigma}^2\alpha_2 + \hat{\sigma}^3\alpha_3 + \ldots.$$

It turns out that α_0, α_1 and α_2 are purely real quantities, and α_3 is the first term to have a non-zero imaginary part. In other words, the growth rate of these instability modes is $O(\hat{\sigma}^4)$, which exceeds the viscous growth rate of the lower-branch T–S modes when $\hat{\sigma} \gg R^{-1/32}$. To facilitate the subsequent study of the nonlinear development of the above modes, we choose to absorb both amplitude and phase variations at the level of α_3 into an amplitude function that varies on the scale

$$X = \hat{\sigma}^4 R^{1/2}\bar{x} = O(1). \tag{2.27}$$

Since X is also much faster than $\bar{x}$ according to (2.21) and (2.23), the space and time modulation of the distortion can be treated as parametric when the stability of the perturbed flow is studied, that is, the disparity between the length and time scales of the instability modes and those of the background flow allows us to seek 'local instability modes' by freezing the instantaneous profile of the latter at a particular time and streamwise location. The term 'eigenfunction' is to be understood in this local sense. The time-scale disparity implies that the global periodicity of the background flow is of little relevance. Nevertheless, a possible connection between the instantaneous instability and the global instability of Floquet type will be discussed in §6.

3. Linear instability analysis

As in Part 1, the linear instability problem is governed by a five-zoned asymptotic structure. In the present problem, however, the Klebanoff distortion in the main deck plays a crucial role in determining the spanwise mode shape. In contrast, the relatively strong distortion in the wall region alone was found to control both the mode shape and the growth rate for the case analysed in Part 1.

The appropriate transverse variable in the main part of the boundary layer corresponds to

$$\hat{y} = \frac{\Lambda R^{1/2}}{l^*} y = (2\bar{x})^{1/2}\eta.$$

The total streamwise velocity of the base flow is then given by

$$U_B + \hat{\sigma} U_D(\hat{y}, Z; \bar{x}, \bar{t}), \tag{3.1}$$

where U_D denotes the normalized distortion profile. For the most part, we shall focus on the case of a time-harmonic free-stream disturbance, for which $U_D = -w_s'(Z)(\bar{U}\,\mathrm{e}^{-\mathrm{i}\bar{t}} + \text{c.c.})$. However, the linear instability analysis presented in this section is also applicable to broadband free-stream disturbances. The eigensolutions in the main deck take the usual form

$$u = \epsilon\{A(X)\Phi(Z)\hat{u}_0(\hat{y}) + \hat{\sigma}\hat{u}_1 + \hat{\sigma}^2\hat{u}_2 + \hat{\sigma}^3\hat{u}_3 + \dots\}\,\mathrm{e}^{\mathrm{i}\zeta} + \text{c.c.}, \tag{3.2}$$

$$v = \epsilon\hat{\sigma}\{A(X)\Phi(Z)\hat{v}_0(\hat{y}) + \hat{\sigma}\bar{v}_1 + \hat{\sigma}^2\hat{v}_2 + \hat{\sigma}^3\hat{v}_3 + \dots\}\,\mathrm{e}^{\mathrm{i}\zeta} + \text{c.c.}, \tag{3.3}$$

$$w = \epsilon\hat{\sigma}^{3/2}\{A(X)\Phi'(Z)\hat{w}_0(\hat{y}) + \hat{\sigma}\hat{w}_1 + \hat{\sigma}^2\hat{w}_2 + \hat{\sigma}^3\hat{w}_3 + \dots\}\,\mathrm{e}^{\mathrm{i}\zeta} + \text{c.c.}, \tag{3.4}$$

$$p = \epsilon\hat{\sigma}\{A(X)\Phi(Z)\hat{p}_0(\hat{y}) + \hat{\sigma}\hat{p}_1 + \hat{\sigma}^2\hat{p}_2 + \hat{\sigma}^3\hat{p}_3 + \dots\}\,\mathrm{e}^{\mathrm{i}\zeta} + \text{c.c.}, \tag{3.5}$$

where ϵ represents the amplitude of the streamwise velocity fluctuation associated with the eigenmodes, and the (normalized) amplitude function $A(X)$ illustrates the growth (or decay) of the eigenmode in the streamwise direction. Here, the terms of $O(\hat{\sigma}^3\log\hat{\sigma})$ in the expansion have not been written out explicitly since they are 'passive' in the sense that matching at this order is automatically guaranteed.

The leading-order terms in the expansions (3.2)–(3.5) have the familiar solution

$$\hat{u}_0 = U_B', \quad \hat{v}_0 = -\mathrm{i}\alpha_0 U_B, \quad \hat{p}_0 = P_0, \quad \hat{w}_0 = -(\mathrm{i}\alpha_0)^{-1}P_0 U_B^{-1}, \tag{3.6}$$

where P_0 is a constant. The second-order terms satisfy

$$\left.\begin{aligned} &\mathrm{i}\alpha_0\hat{u}_1 + \hat{v}_1' = -\mathrm{i}\alpha_1 U_B' A\Phi, \\ &\mathrm{i}\alpha_0 U_B\hat{u}_1 + U_B'\hat{v}_1 = -\mathrm{i}\alpha_0 P_0 A\Phi - \mathrm{i}(\alpha_1 U_B - \omega)U_B' A\Phi - R_s, \\ &\alpha_0^2 U_B^2 A\Phi = -\bar{p}_1', \end{aligned}\right\} \tag{3.7}$$

where primes denote differentiation with respect to $\hat{y}$ and the forcing term

$$R_s = (\mathrm{i}\alpha_0\hat{u}_0 U_D + \hat{v}_0 U_D')A\Phi = \mathrm{i}\alpha_0(U_B' U_D - U_B U_D')A\Phi \tag{3.8}$$

arises from the interaction between the instability wave and the distortion. The solution to (3.7) is found to be

$$\hat{v}_1 = -\mathrm{i}\alpha_0\Phi_1 U_B + \left\{\mathrm{i}\omega + \mathrm{i}\alpha_0 P_0 U_B\int^{\hat{y}}\frac{\mathrm{d}\hat{y}}{U_B^2} - \mathrm{i}\alpha_0 U_D\right\}A\Phi, \tag{3.9}$$

$$\hat{u}_1 = \Phi_1 U_B' + \left\{-\frac{\alpha_1}{\alpha_0}U_B' - P_0\left\{U_B'\int^{\hat{y}}\frac{\mathrm{d}\hat{y}}{U_B^2} + \frac{1}{U_B}\right\} + U_D'\right\}A\Phi, \tag{3.10}$$

$$\hat{p}_1 = \tilde{P}_1 - \alpha_0^2 A\Phi\int_0^{\hat{y}} U_B^2\,\mathrm{d}\hat{y}, \tag{3.11}$$

where Φ_1 and $\tilde{P}_1$ are unknown functions of Z that represent the complementary solution to the system (3.7). The inner limits (i.e. $\hat{y} \to 0$) of (3.9) and (3.10)

are given by

$$\hat{v}_1 \to \mathrm{i}\left(\omega - \frac{\alpha_0}{\lambda}P_0\right)A\Phi - \{\mathrm{i}\alpha_0\Phi_1\lambda + \mathrm{i}\alpha_0(\lambda_D - \lambda J_0 P_0)A\Phi\}\hat{y}, \tag{3.12}$$

$$\hat{u}_1 \to \Phi_1\lambda + \left(-\frac{\alpha_1}{\alpha_0}\lambda + \lambda_D - \lambda J_0 P_0\right)A\Phi, \tag{3.13}$$

respectively, where $\lambda \equiv 0.33206\,\bar{x}^{-1/2}$ denotes the local wall shear of the Blasius flow; and

$$\lambda_D(Z;\bar{x},\bar{t}) \equiv U_D'(0,Z;\bar{x},\bar{t}) = (2\bar{x})^{-1/2}w_s'(Z)(\bar{U}'(0;\bar{x},\bar{t})\,\mathrm{e}^{-\mathrm{i}\bar{t}} + \mathrm{c.c.}) \tag{3.14}$$

represents the instantaneous wall-shear perturbation due to the Klebanoff fluctuation. The constant J_0 is defined by

$$J_0 = -\int_0^a \left(\frac{1}{U_B^2} - \frac{1}{\lambda^2\hat{y}^2}\right)\mathrm{d}\hat{y} + \frac{1}{\lambda^2 a^2},$$

where a is an arbitrary constant.

In the upper-deck region corresponding to $\bar{y} \equiv \hat{\sigma}\,\hat{y} = O(1)$, it is adequate to consider the solution for the perturbation in pressure and vertical velocity. These expand as

$$\left.\begin{aligned} p &= \epsilon\hat{\sigma}\left\{A(X)\Phi(Z)\bar{p}_0 + \hat{\sigma}\,\bar{p}_1 + \hat{\sigma}^2\bar{p}_2 + \hat{\sigma}^3\bar{p}_3 + \ldots\right\}\mathrm{e}^{\mathrm{i}\zeta} + \mathrm{c.c.},\\ v &= \epsilon\hat{\sigma}\left\{A(X)\Phi(Z)\bar{v}_0 + \hat{\sigma}\,\bar{v}_1 + \hat{\sigma}^2\bar{v}_2 + \hat{\sigma}^3\bar{v}_3 + \ldots\right\}\mathrm{e}^{\mathrm{i}\zeta} + \mathrm{c.c.} \end{aligned}\right\} \tag{3.15}$$

The leading-order pressure perturbation $\bar{p}_0$ and the first-order correction $\bar{p}_1$ are governed by

$$\bar{p}_{0,\bar{y}\bar{y}} - \alpha_0^2\bar{p}_0 = 0, \quad \bar{p}_{1,\bar{y}\bar{y}} - \alpha_0^2\bar{p}_1 = (2\alpha_0\alpha_1\Phi - \Phi_{ZZ})A\bar{p}_0,$$

which yield the solutions

$$\bar{p}_0 = P_0\,\mathrm{e}^{-\alpha_0\bar{y}}, \quad \bar{p}_1 = \bar{P}_1(X,Z)\,\mathrm{e}^{-\alpha_0\bar{y}} + A\left(-\alpha_1\Phi + \frac{1}{2\alpha_0}\Phi_{ZZ}\right)P_0\bar{y}\,\mathrm{e}^{-\alpha_0\bar{y}}. \tag{3.16}$$

The corresponding solution for the vertical velocity fluctuation can be easily derived from the vertical momentum equation,

$$\mathrm{i}\alpha_0\bar{v}_0 = -\bar{p}_0', \quad \mathrm{i}\alpha_0\bar{v}_1 + \mathrm{i}(\alpha_1 - \omega)A\Phi\bar{v}_0 = -\bar{p}_1',$$

which implies the inner behaviour

$$\bar{v}_0 \to -\mathrm{i}P_0, \quad \bar{v}_1 \to -\mathrm{i}\bar{P}_1 + A\left(-\mathrm{i}\frac{\omega}{\alpha_0}\Phi + \frac{\mathrm{i}}{2\alpha_0^2}\Phi_{ZZ}\right)P_0 \quad \text{as} \quad \bar{y} \to 0. \tag{3.17}$$

By matching the upper-deck solutions for pressure and vertical velocity with the outer expansions of the main-deck solutions ((3.9) and (3.11)), we obtain

$$\bar{P}_1 = \tilde{P}_1 - \alpha_0^2 I_2 A\Phi, \tag{3.18}$$

$$-\mathrm{i}\bar{P}_1 + \left(-\mathrm{i}\frac{\omega}{\alpha_0}A\Phi + \frac{\mathrm{i}}{2\alpha_0^2}\Phi_{ZZ}\right)P_0 = -\mathrm{i}\alpha_0 A\Phi_1 + (\mathrm{i}\omega + \mathrm{i}\alpha_0 J_\infty P_0)A\Phi, \tag{3.19}$$

where

$$I_2 = \int_0^\infty U_B^2\,\mathrm{d}\hat{y}, \quad J_\infty = \int_a^\infty \left(\frac{1}{U_B^2} - 1\right)\mathrm{d}\hat{y}.$$

The main-deck expansions (3.2)–(3.5) become non-uniform as $\hat{y} \to 0$ and one must, therefore, consider the Tollmien layer defined by

$$Y = \hat{y}/\hat{\sigma} = O(1),$$

where the base flow can be approximated by the McLaurin expansion of (3.1),

$$\hat{\sigma}(\lambda + \hat{\sigma}\lambda_D)Y + \hat{\sigma}^4\left(-\frac{\lambda^2}{48}Y^4 + U_D'''(0, Z; \bar{x}, \bar{t})Y^3\right) + \ldots. \tag{3.20}$$

Note that the velocity of the Blasius flow is changed only slightly by the distortion, but its curvature is completely altered.

The solution for the instability wave expands as

$$\left.\begin{aligned} u &= \epsilon(A(X)\Phi(Z)\tilde{U}_0 + \hat{\sigma}\tilde{U}_1 + \hat{\sigma}^2\tilde{U}_2 + \hat{\sigma}^3\tilde{U}_3 + \ldots)\,\mathrm{e}^{\mathrm{i}\zeta} + \text{c.c.},\\ v &= \epsilon\hat{\sigma}^2(A(X)\Phi(Z)\tilde{V}_0 + \hat{\sigma}\tilde{V}_1 + \hat{\sigma}^2\tilde{V}_2 + \hat{\sigma}^3\tilde{V}_3 + \ldots)\,\mathrm{e}^{\mathrm{i}\zeta} + \text{c.c.},\\ p &= \epsilon\hat{\sigma}(A(X)\Phi(Z)\tilde{P}_0 + \hat{\sigma}\tilde{P}_1 + \hat{\sigma}^2\tilde{P}_2 + \hat{\sigma}^3\tilde{P}_3 + \ldots)\,\mathrm{e}^{\mathrm{i}\zeta} + \text{c.c.} \end{aligned}\right\} \tag{3.21}$$

The leading-order solution is

$$\tilde{U}_0 = \lambda, \quad \tilde{V}_0 = -\mathrm{i}\alpha_0\lambda Y,$$

and matching with the main-deck solution gives $P_0 = \alpha_0$, as well as the leading-order dispersion relation

$$\alpha_0 = (\lambda\omega)^{1/2}. \tag{3.22}$$

The second-order terms in the Tollmien layer are governed by

$$\mathrm{i}\alpha_0\tilde{U}_1 + \tilde{V}_1' = -\mathrm{i}\alpha_1\lambda A\Phi,$$
$$\mathrm{i}(\alpha_0\lambda Y - \omega)\tilde{U}_1 + \lambda\tilde{V}_1 = -\mathrm{i}\alpha_0\tilde{P}_1 - \mathrm{i}\alpha_1 P_0 A\Phi - \mathrm{i}\alpha_1\lambda^2 A\Phi Y.$$

The matching requirement with the small-y asymptote of the main-deck solution (3.12)–(3.13) suggests that $\tilde{U}_1$ and $\tilde{V}_1$ must have the solution

$$\left.\begin{aligned} \tilde{U}_1 &= \Phi_1\lambda + (-\alpha_1/\alpha_0)\lambda + \lambda_D - \lambda J_0 P_0)A\Phi,\\ \tilde{V}_1 &= \{-\mathrm{i}\alpha_0\Phi_1\lambda + \mathrm{i}\alpha_0(\lambda_D - \lambda J_0 P_0)A\Phi\}Y. \end{aligned}\right\} \tag{3.23}$$

The above solution satisfies the continuity equation and substituting it into the momentum equation yields the constraint

$$\omega\lambda\left\{\Phi_1 + \left(-\frac{\alpha_1}{\alpha_0} + \frac{\lambda_D}{\lambda} - J_0 P_0\right)A\Phi\right\} = \alpha_0\tilde{P}_1 + \alpha_1 P_0 A\Phi. \tag{3.24}$$

It follows from relations (3.18), (3.19), (3.22) and (3.24) that the spanwise mode shape $\Phi(Z)$ is governed by the Schrödinger equation

$$\Phi_{ZZ} + (\psi(Z; \bar{x}, \bar{t}) - \alpha_s)\Phi = 0, \tag{3.25}$$

where we have set

$$\psi(Z; \bar{x}, \bar{t}) = \frac{2\lambda_D(Z)\alpha_0^2}{\lambda} = -\frac{2\alpha_0^2}{(2\bar{x})^{1/2}\lambda}(\bar{U}'\,\mathrm{e}^{-\mathrm{i}\bar{t}} + \text{c.c.})w_s'(Z) \equiv -\tilde{\psi}(\bar{x}, \bar{t})w_s'(Z), \tag{3.26}$$

and

$$\alpha_s = 4\alpha_0\{\alpha_1 - \tfrac{1}{2}\alpha_0^2(J_\infty - J_0 - I_2) - \omega\}.$$

Observe that α_s represents the eigenvalue of the Schrödinger operator with a potential function (or 'scatter' in the general sense) corresponding to the distortion $\lambda_D(Z; x, t)$

in the wall skin friction. Even though the interaction between the instability wave and the distortion takes place in the bulk of the flow, the net effect of this interaction is fully characterized by a local quantity λ_D with the detailed profile of the distortion being largely irrelevant.

It now transpires that the reason for choosing (2.20) was to ensure a balance between the spanwise variation of the modal shape, Φ_{ZZ}, and the wavenumber correction $\alpha_s\Phi$ in (3.25). Without retaining Φ_{ZZ}, α_s would be parametrically dependent on the spanwise variable Z. Any higher-order terms involving first- and second-order derivatives with respect to Z would lead to secular terms proportional to $\bar{x}$ and $\bar{x}^2$, respectively, which would have invalidated the entire perturbation scheme. An eigenvalue problem analogous to (3.25) was previously obtained by Timoshin & Smith (1997) in the context of purely inviscid singular modes induced by a stationary distortion.

Thus far, we have not made any distinction between local and periodic distortions. In the rest of this section and in the following section, we shall assume that $\lambda_D(Z)$ is localized. However, the main results can be applied to the periodic distortion after rather minor modifications, as discussed in § 5 below. The Schrödinger operator is well-studied and there is extensive literature on the structure of its spectrum. For our purpose, it suffices to mention that for a localized potential, the Schrödinger operator has a discrete spectrum (if the potential is not negative definite), and the eigenfunctions Φ are real valued and decay exponentially as $Z \to \pm\infty$. In this paper, we normalize the eigenfunction such that

$$\int_{-\infty}^{\infty} \Phi^2 \, \mathrm{d}Z = 1.$$

There also exists a continuous spectrum such that Φ remains finite and oscillatory at $Z \to \pm\infty$. However, only the discrete spectrum will be considered in this paper, with the exception of a few additional comments on the possible relevance of the continuum modes.

The analysis can be carried to higher orders in a routine manner (cf. Wu, Stewart & Cowley 1996). Consideration of the third terms in the expansion for each deck determines α_2, but the details of this calculation, as well as α_2 itself, are of little relevance here and hence are omitted. The crucial equation, which determines the modal growth rate, is obtained by considering the fourth term in the expansion for each deck. The final result is

$$-\frac{\mathrm{i}}{4\alpha_0}\Phi_{2,ZZ} = \frac{\mathrm{i}}{4\alpha_0}\left\{\frac{2\lambda_D(Z)\alpha_0^2}{\lambda} - \alpha_s\right\}\Phi_2 - A_X\Phi + (\gamma_0 + \gamma(Z))A\Phi + \mathrm{i}\chi(Z, X), \qquad (3.27)$$

where the function $\Phi_2(X, Z)$ represents the complementary part of the solution for $\tilde{U}_2$ and $\tilde{V}_2$, analogous to Φ_1 in (3.23). The constant γ_0 is defined by

$$\gamma_0 = -\frac{\pi c_0^4}{4\lambda} + \frac{\lambda^2}{2R^{1/4}\hat{\sigma}^5(2\alpha_0 c_0)^{1/2}},$$

while $\gamma(Z;\bar{x},\bar{t})$ corresponds to

$$\gamma(Z;\bar{x},\bar{t}) = -\frac{\pi c_0^3}{\lambda^2}U_D'''(0, Z;\bar{x}, t)(2\bar{x})^{-3/2}\{\bar{U}'''(0;\bar{x})\,\mathrm{e}^{-\mathrm{i}\bar{t}} + \text{c.c.}\}w_s'(Z) \equiv -\tilde{\gamma}(\bar{x},\bar{t})w_s'(Z). \qquad (3.28)$$

The function χ is real-valued and therefore does not affect the leading-order growth rate.

Equation (3.27) is an inhomogeneous Schrödinger equation. The standard procedure of imposing the solvability condition yields

$$A_X = (\gamma_0 + \kappa_d)A,$$

where

$$\kappa_d = \int_{-\infty}^{\infty} \gamma(Z)\Phi^2 \, \mathrm{d}Z. \tag{3.29}$$

The total growth rate therefore corresponds to $(\gamma_0 + \kappa_d)$, with κ_d being the 'excess growth rate' induced by the distortion. When $\hat{\sigma} \gg O(R^{-1/20})$, the excess growth rate becomes much larger than the second term in γ_0, which corresponds to the viscous contribution to the growth rate (Goldstein & Durbin 1986). In other words, the instability modes of interest now become predominantly inviscid, with a growth rate given by

$$\kappa = -\frac{\pi c_0^4}{4\lambda} + \int_{-\infty}^{\infty} \gamma(Z)\Phi^2 \, \mathrm{d}Z. \tag{3.30}$$

In this sense, the nature of the instability has been fundamentally altered by the distortion at this stage. As the distortion amplitude is increased further, the inviscid growth rate continues to increase and for $\hat{\sigma} \gg O(R^{-1/32})$ it exceeds the growth rate of the longer-wavelength lower-branch modes (which are described by the triple-deck structure and correspond to the most unstable modes of the unperturbed flow). It should be noted that though the lower-branch T–S modes have a larger growth rate, they evolve through a relatively small streamwise region (Goldstein & Durbin 1986) so that the contribution of the lower-branch regime to the overall integral growth is asymptotically smaller than that from the upper-branch regime (Cowley & Wu 1994). It may therefore be argued that transition would be primarily caused by inviscid instability provided that $\hat{\sigma} \gg O(R^{-1/20})$.

In summary, we have seen that the asymptotic regime studied above describes a continuous transition as the distortion amplitude is varied, from a modified form of the short-wavelength viscous modes in an unperturbed Blasius flow, to primarily inviscid modes that eventually dominate the overall instability of the perturbed flow. Because the structure of these modes can be localized in the spanwise direction and, in general, is completely dictated by the shape of the Klebanoff distortion, these modes may be referred to as 'localized Rayleigh modes'.

It may be seen from (3.25) and (3.30) that the spanwise shape and the growth rate of the instability mode are controlled, respectively, by the wall shear $U_D'(0, Z; \bar{x}, \bar{t})$ and the torsion $U_D'''(0, Z; \bar{x}, \bar{t})$ of the distortion in the streamwise velocity profile. For a time-harmonic gust, the latter is given by

$$U_D'''(0, Z; \bar{x}, t) = (2\bar{x})^{-3/2}\{\bar{U}'''(0, Z; \bar{x})\, \mathrm{e}^{-\mathrm{i}\bar{t}} + \text{c.c.}\} w_s'(Z), \tag{3.31}$$

which, in view of (2.16), is related to the wall-shear distortion $U_D'(0, Z; \bar{x}, \bar{t})$ via

$$U_D'''(0, Z; \bar{x}, \bar{t}) = U_D'\big(0, Z; \bar{x}, \bar{t} + \tfrac{1}{2}\pi\big).$$

However, as pointed out before, the original equations (3.25) and (3.29) governing the instability modes are valid for any arbitrary form of time dependence for the free-stream gust as long as the asymptotic scalings outlined in § 2.2 are satisfied.

Watmuff (1998) observed that when the amplitude of the free-stream disturbance was reduced, transition occurred earlier. This is indeed an anomalous behaviour if the level of the free-stream disturbance is regarded as the relevant control parameter.

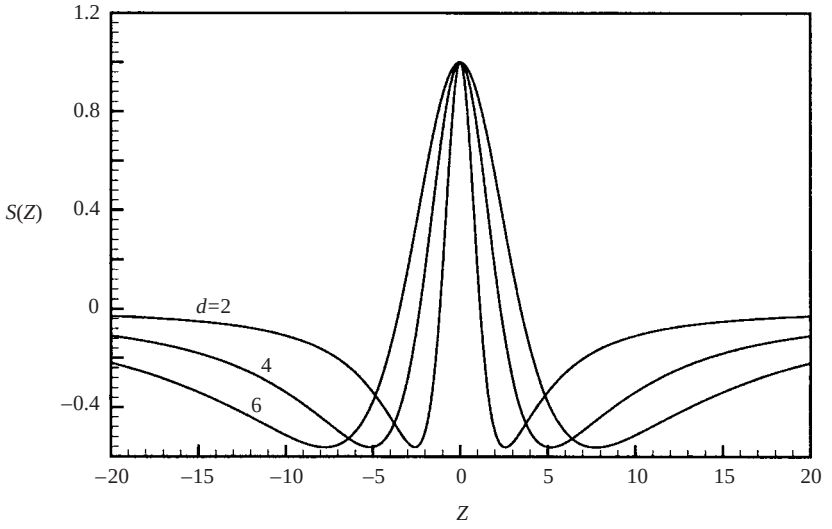

FIGURE 2. The shape of the distortion for $d = 2, 4, 6$.

However, Watmuff also pointed out that the decrease in distortion amplitude was accompanied by the location of its maximum moving closer to the wall; so it is quite possible that the wall-shear perturbation $U'_D(0, Z; \bar{x}, \bar{t})$ increased in magnitude during that process. If that was true, then the seemingly anomalous observation would be completely 'normal' according to the present theory. Unfortunately, the wall-shear perturbation was not measured in Watmuff's experiment and is cumbersome to measure, in general. Therefore, the above conjecture cannot be easily verified.

The spectrum of the Schrödinger operator is well-understood; but, in order to aid our subsequent discussions, we first present solutions for a Klebanoff distortion with the spanwise distribution

$$B(Z) = \frac{d^3 Z}{Z^2 + d^2}, \tag{3.32}$$

where d is a constant. A localized distribution of this type is believed to be appropriate for Klebanoff distortions with a finite correlation distance in Z, but periodic distributions (corresponding to large coherence in Z) can also be easily analysed as discussed in § 5.1 below. Substituting for $B(Z)$ into (2.8) and evaluating the principal-value integral, we find that

$$-w'_s(Z) = \frac{B_0(1 - 3Z^2/d^2)}{(Z^2/d^2 + 1)^3} \equiv B_0 S(Z), \tag{3.33}$$

where we have set $B_0 = 2\pi\hat{v}_\infty$. The shape function $S(Z)$ is depicted in figure 2 for several values of d. The requirement that the spanwise velocity of the distortion vanishes at $\pm\infty$ dictates that $S(Z)$ must change its sign in the spanwise direction. All of the calculations presented below pertain to the (arbitrary) choice of $d = 4$.

Just to illustrate the general behaviour of the spectrum, we first set $\tilde{\psi} = 1$ in (3.26) and plot the eigenvalues α_s for a range of B_0 (figure 3). The variation of B_0 also emulates various instances during a single period of the time-harmonic Klebanoff fluctuation. Specifically, during the modulation phase in which the distortion is characterized by a low-speed streak, the corresponding B_0 is negative. Symmetric (varicose) modes can be found for both positive and negative B_0, except in a gap

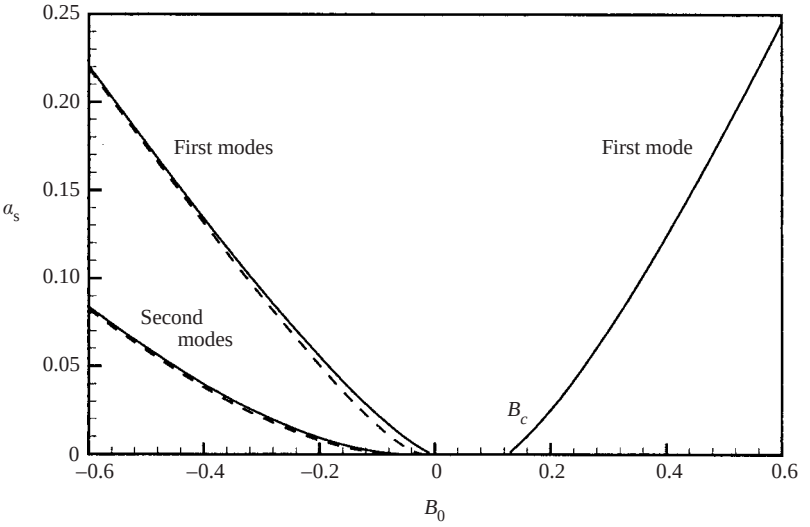

FIGURE 3. Eigenvalues α_s vs. B_0: —, varicose modes; - - -, sinuous modes.

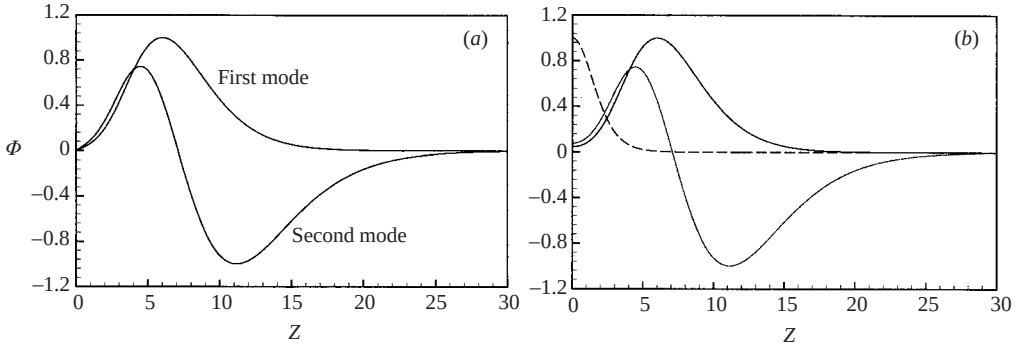

FIGURE 4. Eigenfunctions of the first and second modes for the localized Klebanoff distortion defined by (3.33): sinuous mode (*a*) and varicose mode (*b*) for $d = 4$ and $B_0 = -1$. For comparison, the dashed line represents the eigenfunction of the varicose mode for $d = 4$ and $B_0 = 1$.

$0 < B_0 < 0.16 = B_c$. Unlike the Schrödinger operator with a purely imaginary potential (i.e. the case analysed in Part 1), the standard Schrödinger equation (3.25) also admits antisymmetric (i.e. sinuous) modes in addition to the varicose ones. These modes appear only for negative B_0 (or, equivalently, in a small window that does not exceed one half of the modulation cycle in terms of duration). For $B_0 < 0$, there are also higher unstable modes, both symmetric and antisymmetric, which are distinguished by the number of zeros in the corresponding eigenfunctions, as displayed in figures 4(*a*) and 4(*b*). These higher modes are generally less unstable than the first ones and, accordingly, will not be discussed here any further. While the symmetric modes for $B_0 > B_c$ concentrate near the centreline (see the dashed line in figure 4*b*), the modes for $B_0 < 0$ have peaks outside the main region of the mean-flow distortion. Interestingly, the eigenvalue α_s and the eigenfunctions $\Phi(Z)$ for the varicose and sinuous modes for $B_0 < 0$ are remarkably similar to each other (except in the immediate vicinity of $Z = 0$) in this particular case, as seen from figures 3 and 4.

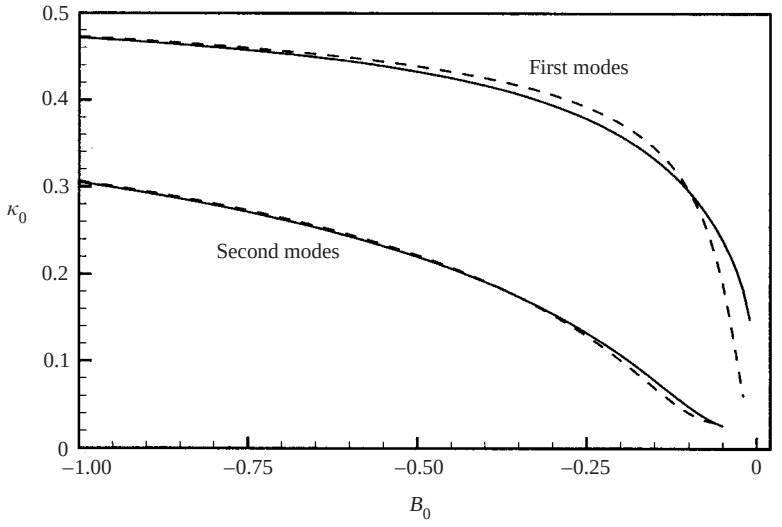

FIGURE 5. Variation of the 'unit growth rate' with B_0. —, Varicose modes; - - -, sinuous modes.

To assess the relative importance of the sinuous and the varicose modes, we now examine the 'unit growth rate', which is defined as

$$\kappa_0 = -\int_{-\infty}^{\infty} S(Z)\Phi^2 \, \mathrm{d}Z$$

and, therefore, represents the excess growth rate (3.29) normalized by the amplitude of the distortion. As is shown in figure 5, the first sinuous modes exhibit a slightly higher unit growth rate than the varicose modes, except as $B_0 \to 0$ when the growth rate κ_0 decreases sharply.

Equations (3.25), (3.26) and (3.28) are used in conjunction with (3.30) to compute the inviscid growth rate due to the time-varying Klebanoff distortion. The growth rates of both the sinuous and varicose modes at three separate instants of time are shown in figure 6 for the case of $\bar{x} = 2.0$ and $B_0 = 1.4$. Observe that the sinuous modes have considerably larger growth rates than the varicose modes. For this reason, we shall focus on the sinuous modes henceforth. Indeed, even in the experiments of Matsubara & Alfredsson (2001), the sinuous modes were noted to occur more frequently.

As described earlier in the context of figure 3, sinuous modes exist only when $\tilde{\psi}(\bar{x}, \bar{t})$ is negative, i.e. at those instants during the modulation cycle when the perturbed flow is characterized by a significant low-speed streak. This finding is consistent with many of the experimental observations noted in the Introduction. Furthermore, the instability occurs only in that part of cycle when $\tilde{\gamma}(\bar{x}, \bar{t})$ is also negative. On the other hand, γ and ψ tend to 0 as both $\bar{x} \to 0$ and $\bar{x} \to \infty$; the former is implied by (2.15), while the latter is apparent from figure 1. Thus, γ and ψ have appreciable magnitudes only over a restricted window in the streamwise direction. The instability modes under consideration are, therefore, expected to be localized in space as well as in time.

The local and intermittent nature of the instability can be further illustrated by plotting the growth-rate contours in the (ω, $\bar{x}$)-plane at various instants of time, as shown in figure 7(*a–d*) for the case of $B_0 = 1.4$. At $\bar{t} = -1.8$, a small 'bubble' of instability is observed within the (ω, $\bar{x}$)-plane, indicating the instigation of the

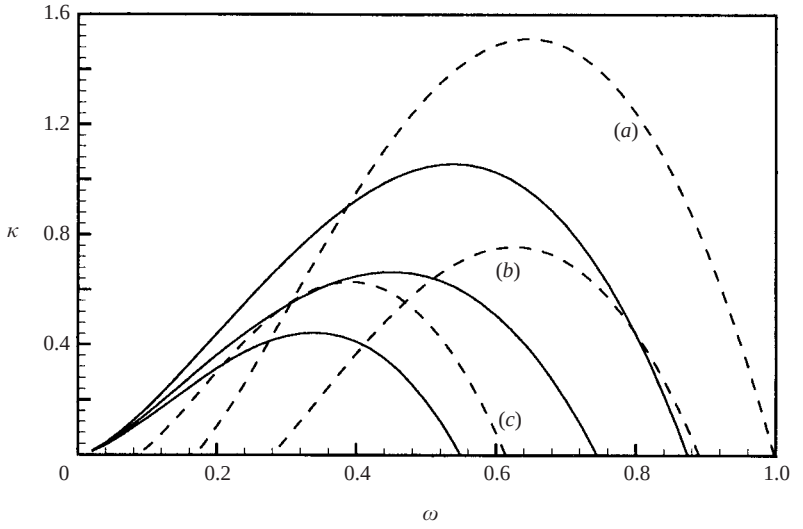

FIGURE 6. Instability caused by a Klebanoff distortion. The streamwise location is fixed at $\bar{x} = 2.0$ and $B_0 = 1.4$. The growth rates of varicose (—) and sinuous modes (- - -) at three instants: (*a*) $\bar{t} = \phi(x) - \frac{3}{4}\pi$; (*b*) $\bar{t} = \phi(x) - \frac{7}{8}\pi$; (*c*) $\bar{t} = \phi(x) - \frac{29}{32}\pi$, where $\phi(\bar{x}) \approx 2.31$ denotes the local phase of the wall torsion $\bar{U}'''(0, \bar{x})$.

instability to be at a slightly earlier time. As time increases, the bubble grows in both spatial and spectral extent, reaching its maximum at $\bar{t} \approx -0.82$, after which the bubble shrinks and finally disappears, before re-emerging during the next cycle of the Klebanoff fluctuation. Of course, given the disparity between the temporal scales of the Klebanoff fluctuation and the instability waves the latter could amplify substantially within a single period of modulation and, therefore, reach sufficiently high amplitudes to induce a local breakdown. For the periodically modulated Klebanoff distortion, the instability occurs during a fixed phase of the cycle, but, in reality, the modulation is stochastic so that this local instability takes place randomly as has been observed in the experiments of Kendall (1985).

It is possible to make certain deductions about the spatio-temporal behaviour of the instability from figure 7(*a–d*). The localized structure of the instability wave in both x and Z suggests that, in practice, the instability collectively would be manifested as patches of oscillations. Since unlike usual T–S wavepackets, a patch of relatively high-frequency disturbances cannot be sustained in an undistorted region; they must therefore concentrate in the region where the distorted flow is unstable. The apparent downstream migration of the unstable region therefore implies convection of oscillation patches. The precise shape of the patches and their convection velocity, however, could only be determined after considering the complex history of all unstable disturbances in a distorted flow. These are left for further investigation.

It is expected that the unstable modes might amplify sufficiently over a single cycle of modulation to unleash a chain of nonlinear events, which we now describe.

4. Nonlinear instability

The linear stability analysis in the previous section was based on the assumption that the amplitude ϵ of the instability waves is sufficiently small. However, as the waves are amplified and attain a certain threshold range of amplitudes, the nonlinear

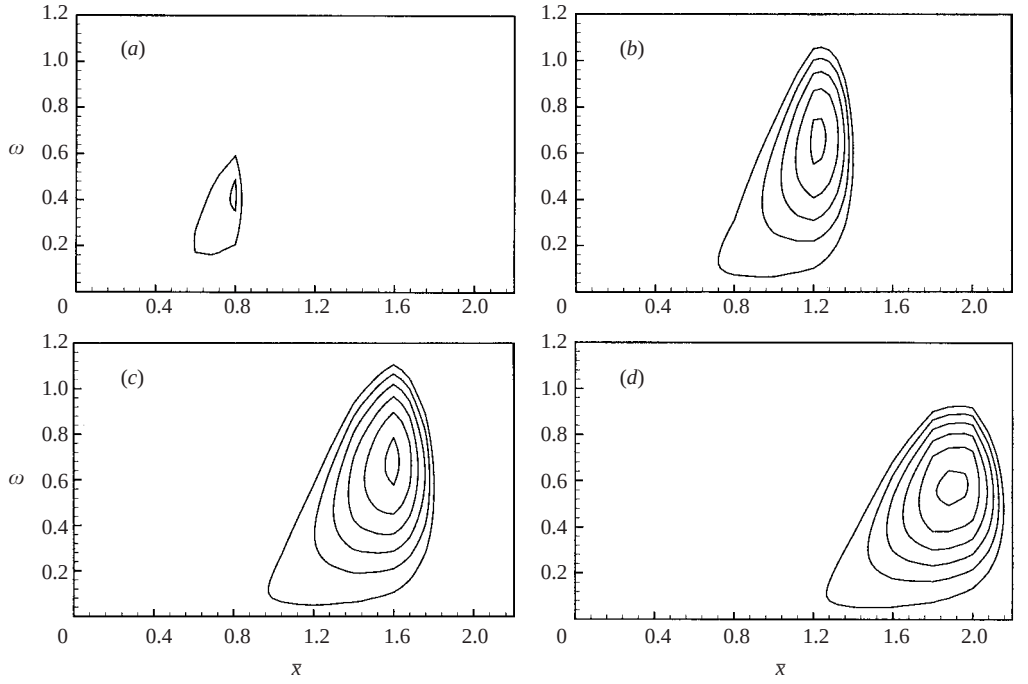

FIGURE 7. Contours of growth rates of the local instability induced by a Klebanoff mode ($B_0 = 1.4$) at the instants (*a*) $\bar{t} = -1.8$, (*b*) -1.25, (*c*) -0.82, (*d*) -0.44.

effects also become significant. In this section, we will show that the instability waves evolve through two distinct weakly nonlinear stages before finally entering the strongly nonlinear regime of development. To a great extent, the details of this nonlinear analysis are similar to the previous analyses of non-equilibrium critical layers; therefore, many of the details related to this analysis are omitted.

4.1. *Nonlinear stage I*

The first nonlinear stage is attained when

$$\epsilon = O(\hat{\sigma}^{19/2}) \sim \left(\frac{\Lambda R_\Lambda}{l^*}\right)^{-19/6}. \tag{4.1}$$

At this stage, the fluctuations associated with the instability wave still expand according to (3.2)–(3.5), as in the linear case. Moreover, the first three terms in the expansions are unaffected by nonlinearity so that the shape of the spanwise eigenfunction $\Phi(Z)$ continues to be governed by (3.25). It is now well-established that the dominant nonlinear interaction occurs within the critical layer and the effect of this cubic nonlinearity is to produce a velocity jump N across this layer (Goldstein 1994; Cowley & Wu 1994). The disturbance amplitude in (4.1) was chosen so that this jump influences the overall development (i.e. growth) of the instability mode at the same order as the linear dynamics.

The form of the nonlinear term depends on viscous effects. As in Part 1, we assume that

$$R^{-1/2} = r\hat{\sigma}^{13},$$

where the Haberman (1972) parameter r ($r = O(1)$) characterizes the relative influence of viscosity with respect to nonlinearity within the critical layer.

The jump N is given by the same expression as (5.3) in Part 1, provided that $A(X)$ in that equation is replaced by the combined mode shape $A(X)\Phi(Z)$. Of course, the Z-dependent factors can now be brought outside of the integral sign. Again, matching the solution from each deck to the respective solutions from the adjacent regions yields (3.27), but with the nonlinear velocity jump N added to the right-hand side. Applying the solvability condition to this inhomogeneous equation, we obtain the nonlinear amplitude evolution equation

$$A_X = \kappa A - \mathrm{i}\Gamma \int_0^\infty \int_0^\infty \xi^2(2\xi+\eta)K(\xi,\eta|s)A(X-\xi)A(X-\xi-\eta)A^*(X-2\xi-\eta)\,\mathrm{d}\xi\,\mathrm{d}\eta, \tag{4.2}$$

where

$$\Gamma = 2\pi\lambda^3\alpha_0^5 c^4 \int_{-\infty}^\infty (\Phi\Phi_Z)^2\,\mathrm{d}Z, \quad K(\xi,\eta|s) = \exp -s(2\xi^3+3\xi^2\eta), \quad s = \tfrac{1}{3}\alpha_0^2\lambda^2 r. \tag{4.3}$$

The appropriate initial condition for (4.2) follows from matching the upstream behaviour of the nonlinear solution with the linear stage, namely

$$A \to \mathrm{e}^{\kappa X} \quad \text{as} \quad x \to -\infty. \tag{4.4}$$

Numerical solutions presented below demonstrate that, for relatively weak viscosity (i.e. $r \ll 1$), $A(X)$ develops a singularity at a finite location X_s, and that the structure of this singularity is the same as that proposed earlier by Goldstein & Choi (1989):

$$A(X) \sim \frac{a_0}{(X_s - X)^{3+\mathrm{i}q}} \quad \text{as} \quad X \to X_s, \tag{4.5}$$

where q is a real number. The above singularity, however, does not occur when the viscous parameter s exceeds a critical value.

Equation (4.2) is formally derived by assuming that $r = O(1)$. However, the permissible range of r is in fact quite large,

$$R_\Lambda^{-1} \leqslant r \leqslant R_\Lambda^{6/23},$$

as may be deduced from (2.17), (2.21) and (2.23). Thus, r (or, equivalently, s) can be either a small or a large parameter without invalidating (4.2). The simplified form of this evolution equation in the very viscous limit $s \to \infty$ can be derived by rescaling the amplitude function according to

$$A = s^{7/8}\hat{A}(X)\big(\exp \mathrm{i}s^{1/4}\Theta\big). \tag{4.6}$$

Inserting this into the nonlinear term in (4.2), and performing integration by parts, we obtain

$$\begin{aligned} N = (6s)^{-1} \int_0^\infty \int_0^\infty & K(\xi,\eta)\{1 - s^{1/4}\xi[\Theta'(X-\xi) + \Theta'(X-\xi-\eta) - 2\Theta'(X-2\xi-\eta)]\} \\ & \times \exp\big\{\mathrm{i}s^{1/4}[\Theta(X-\xi) + \Theta(X-\xi-\eta) + \Theta(X-2\xi-\eta)]\big\} \\ & \times \hat{A}(X-\xi)\hat{A}(X-\xi-\eta)\hat{A}^*(X-2\xi-\eta)\,\mathrm{d}\xi\,\mathrm{d}\eta + \ldots, \end{aligned} \tag{4.7}$$

where we have ignored the terms which do not affect the first two orders of the asymptote for N. As in Wu *et al.* (1996), we now introduce the substitution $\xi \to s^{-1/2}\xi$, and take the limit $s \to \infty$ to obtain a two-term asymptotic approximation for N.

Inserting this, along with (4.6), into (4.2), we find that

$$\left.\begin{aligned} \Theta' &= \frac{(3\pi)^{1/2}}{72}\Gamma\int_0^\infty \eta^{-1/2}|\hat{A}(X-\eta)|^2\,\mathrm{d}\eta, \\ \hat{A}' &= \kappa\hat{A} + \frac{\Gamma}{36}\hat{A}\int_0^\infty \eta^{-1}[\Theta'(X)-\Theta'(X-\eta)]|\hat{A}(X-\eta)|^2\,\mathrm{d}\eta. \end{aligned}\right\} \tag{4.8}$$

The first of these equations indicates that nonlinearity induces a wavelength shortening or 'dilation', which in turn influences the modulus of the disturbance amplitude via the coupling between the phase and the amplitude equations. The energy growth is now governed by an equation with a quintic nonlinearity, as may be verified by substituting the first equation into the second. An analogous finding was noted earlier by Wu, Leib & Goldstein (1997) in the context of nonlinear interaction between pairs of T–S waves.

4.2. *Nonlinear stage II*

The structure (4.5) of the singularity during stage I of the nonlinear evolution shows that

$$A_X/A \sim (X_s - X)^{-1} \quad \text{as} \quad X \to X_s,$$

which suggests that the instability mode must now evolve over a faster scale in the streamwise direction. In particular, a distinct asymptotic regime is reached when $X_s - X = O(\hat{\sigma}^2)$, because the amplitude growth rate becomes comparable with the $O(\hat{\sigma})$ wavelength correction caused by the Klebanoff distortion. The scaled streamwise coordinate governing this second stage of nonlinear evolution is defined as

$$\tilde{X} = (X - X_s)/\hat{\sigma}^2. \tag{4.9}$$

The disturbance amplitude $\epsilon A(X)$ has increased to $O(\tilde{\epsilon})$, where

$$\tilde{\epsilon} = \epsilon\hat{\sigma}^{-6} = \hat{\sigma}^{7/2}. \tag{4.10}$$

In this regime, the instability-wave perturbations in the main part of the boundary layer expand according to

$$u = \tilde{\epsilon}\{\tilde{A}(\tilde{X}, Z)\bar{u}_0\,\mathrm{e}^{\mathrm{i}\zeta} + \hat{\sigma}u_1 + \ldots\} + \text{c.c.},$$

with similar expansions for v, w and p. Observe that, unlike in the preceding stages of evolution, the growth of the unstable fluctuations is non-uniform across the relevant range of spanwise locations; consequently, the amplitude function $\tilde{A}$ depends on both $\tilde{X}$ and Z.

Matching the solutions in the various decks at the second order of approximation leads to the amplitude equation for $\tilde{A}(\tilde{X}, Z)$:

$$\tilde{A}_{\tilde{X}} - \frac{\mathrm{i}}{4\alpha_0}\tilde{A}_{ZZ} = \frac{\mathrm{i}}{4\alpha_0}(\psi(Z;\bar{x},\bar{t}) - \alpha_s)\tilde{A} + \mathrm{i}\tilde{\Gamma}\tilde{N}(\tilde{X}, Z), \tag{4.11}$$

where $\tilde{\Gamma} = \pi\lambda^3\alpha_0^5 c^4$, and the nonlinear term,

$$\begin{aligned} \tilde{N} = \int_0^\infty\int_0^\infty \{&\xi^3\tilde{A}(X-\xi)\tilde{A}(X-\xi-\eta)\tilde{A}^*_{ZZ}(X-2\xi-\eta) \\ &+ \xi^2\eta\tilde{A}(X-\xi)[\tilde{A}(X-\xi-\eta)\tilde{A}^*_Z(X-2\xi-\eta)]_Z \\ &+ \xi^3[\tilde{A}(X-\xi)\tilde{A}(X-\xi-\eta)\tilde{A}^*_Z(X-2\xi-\eta)]_Z\}\,\mathrm{d}\xi\,\mathrm{d}\eta, \end{aligned} \tag{4.12}$$

again represents the effect of interactions within the critical layer. Because of the shorter streamwise length scale during the second nonlinear stage, the width of the

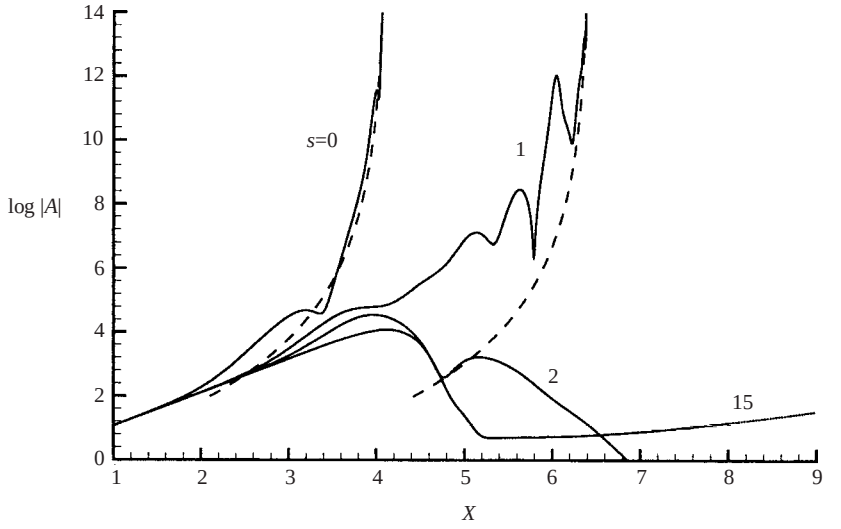

FIGURE 8. Nonlinear evolution of the most unstable (sinuous) mode in figure 7(*b*) ($B_0 = 1.4$, $\hat{x} = 1.2$, $\omega = 0.65$) for viscosity parameter $s = 0$, 1.0, 2.0 and 15.0. The dashed line represents the local singular solution (4.5).

critical layer has increased from an $O(\hat{\sigma}^4)$ value (during the first nonlinear stage) to $O(\hat{\sigma}^2)$. As a result of the thicker critical-layer region, viscous effects no longer play any role in determining the disturbance evolution at the above order.

Equation (4.11) reflects the balance between spanwise scattering by the Klebanoff distortion and the nonlinear effects, while the linear growth has become a secondary effect during stage II. A distinguishing feature of this stage is that the spanwise distribution of the instability wave is altered by the nonlinear effects, in contrast to stage I wherein the spanwise modal shape was independent of the modal amplitude.

The appropriate initial condition for (4.11) follows from the requirement of matching with the singular solution from the upstream region. Thus,

$$\tilde{A} \to a_0(-\tilde{X})^{-(3+iq)}\{\Phi(Z) + (-\tilde{X})^{-1}\Phi_1(Z) + \ldots\}\,\mathrm{e}^{\mathrm{i}\alpha_s \tilde{X}} \quad \text{as} \quad \tilde{X} \to -\infty\,. \tag{4.13}$$

The dominant term on the right-hand side of (4.13) is easily derived by rewriting (4.5) in terms of $\tilde{X}$. The governing equation for the second-order correction term Φ_1 can be obtained by inserting (4.13) into (4.11) and equating the terms at $O((-\tilde{X})^{-4})$. To obtain a unique solution for Φ_1 from this equation, the orthogonality condition,

$$\int_{-\infty}^{\infty} \Phi\Phi_1 \,\mathrm{d}Z = 0,$$

is imposed. Note that the amplitude evolution equation (4.11) for stage II could have been derived without considering the solution from stage I. However, the latter is still essential to derive the initial condition (4.13).

4.3. *Numerical results for nonlinear evolution*

To illustrate the features of amplitude evolution during the nonlinear stage I, we plot the magnitude of A as a function of the streamwise coordinate X (figure 8). The parameter $\bar{x}$, which indicates the streamwise location on the longer streamwise scale, is chosen (somewhat arbitrarily) to be 1.2; similarly, the distortion amplitude is chosen to be $B_0 = 1.4$ and the frequency of the most unstable, i.e. sinuous, mode to be

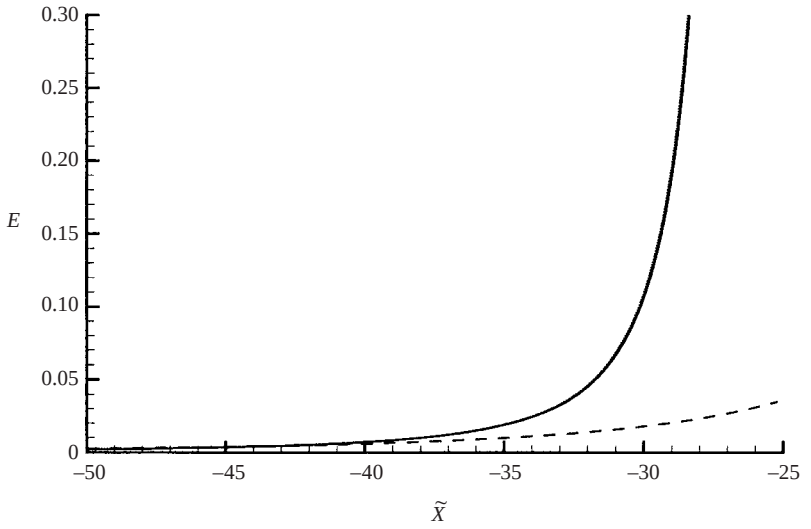

FIGURE 9. Nonlinear evolution in stage II: E vs. $\tilde{X}$.

$\omega = 0.65$. For the purpose of plotting the results, we have renormalized the amplitude function $A(X)$ such that the coefficient $\Gamma = 1$.

As mentioned earlier, the solution develops a singularity of the form (4.5) at sufficiently small values of the viscosity parameter s. Figure 8 shows, however, that the amplification is not monotonic; rather it exhibits transient decay or oscillations before the eventual blowup at a finite distance downstream. It is interesting to note that increasing the viscous effect appears to produce stronger oscillations upstream of the singularity. The amplitude curve for $s = 1$ displays multiple spikes even on the logarithmic scale. These spikes are adequately resolved during the numerical integration process by using a fine step size ($\Delta\tilde{X} = 1/400$). At larger values of the viscosity parameter s (namely at $s = 2$ and $s = 15$), nonlinearity has a stabilizing effect on the disturbance evolution and the solution either decays in a non-monotonic fashion (as at $s = 2$ in figure 8) or amplifies slowly towards the end of the integration domain ($s = 15$).

As noted earlier, the stage I formulation becomes invalid when approaching the singularity and one needs to solve (4.11) to predict the subsequent evolution of the instability mode during stage II of nonlinear evolution. In order to ensure a smooth match with the upstream solution, however, it is necessary to pick a large enough value of $-\tilde{X}$ for imposing the constraint (4.13). To this end, we perform a trial integration through the far-upstream region (typically starting at $\tilde{X} = -250$) so as to identify the region over which the one- and two-term approximations from (4.13) may be considered as being sufficiently accurate. A relatively coarse grid ($\Delta\tilde{X} = 0.5$) is typically adequate for this purpose. Typically, we found that a two-term approximation is accurate up to $\tilde{X} \approx -120$. The solution downstream from this location is obtained by marching (4.11) with a smaller step size. Because the amplitude function now depends on both streamwise and spanwise coordinates, we introduce the norm

$$E(\tilde{X}) = \left\{ \int_{-\infty}^{\infty} |A(Z, \tilde{X})|^2 \, \mathrm{d}Z \right\}^{1/2}$$

to measure the disturbance amplitude at a given streamwise location. Figure 9

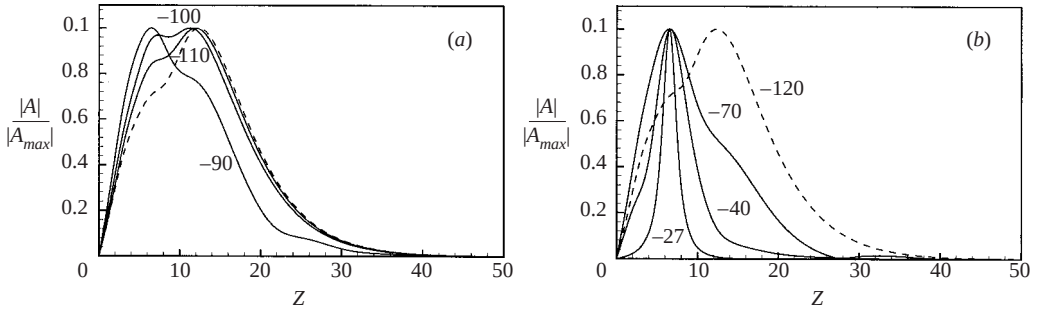

FIGURE 10. Spanwise distribution of $|A|$ at different values of $\tilde{X}$.

illustrates the streamwise development of $E(\tilde{X})$ through the nonlinear stage II. Observe that the simultaneous spatio-temporal modulation during nonlinear stage II has a strong destabilizing effect, which causes an explosive amplification of the disturbance to lead to yet another singularity at a finite distance $\tilde{X}_s$ on the shorter streamwise scale involved. The spanwise distribution of A at three typical streamwise stations is shown in figure 10. As illustrated therein, the nonlinear deformation first leads to a shift in the peak location from $Z \approx 12.0$ to $Z \approx 6.5$, and then to a steepening of the mode shape near the peak at $Z_s \approx 6.5$. Thus, nonlinearity inhibits any lateral spreading and, apparently, leads to a singularity of self-focusing type.

Equation (4.11) is similar to the modulation equation in Wu (1993) with the main difference being the additional (linear) term proportional to $\psi\tilde{A}$. When focusing occurs, this term becomes secondary, and the main balance is between the left-hand-side terms and the nonlinear term on the right-hand side of (4.11). Thus the structure of the self-focusing singularity may be of the same type as that proposed in Wu (1993), namely

$$\tilde{A} = (\tilde{X}_s - \tilde{X})^{-(5/2+ib)} F(\hat{Z}), \quad \hat{Z} = (\tilde{X}_s - \tilde{X})^{-1/2}(Z - Z_s), \tag{4.14}$$

where b is a real constant and F satisfies a rather complex equation given in Wu (1993). If the final outcome of the stage II evolution is represented by (4.14), then the subsequent disturbance evolution must occur on the even shorter scale

$$\tilde{X}_s - \tilde{X} = O(\hat{\sigma}).$$

The growth rate of the disturbance is now comparable with the streamwise wavenumber and the local spanwise length scale (near $Z = Z_s$) is also of the same order as the streamwise wavelength. The appropriate local variables are then given by

$$\hat{X} = (\tilde{X} - \tilde{X}_s)/\hat{\sigma}\ , \quad \hat{Z} = \hat{\sigma}^{-1/2}(Z - Z_s).$$

One also finds that due to a further increase in the thickness of the non-equilibrium critical layer in the new regime, the critical layer actually merges with the Tollmien layer. Since the amplitude of the disturbance increases to $\tilde{\epsilon}\hat{\sigma}^{-5/2} = O(\hat{\sigma})$, i.e. is of the same order as the Blasius flow in the Tollmien layer, the flow in this region becomes strongly nonlinear. In fact, the whole flow is now described by the inviscid form of the fully three-dimensional triple-deck system. Earlier, Wu *et al.* (1997) had shown that pairs of viscous T–S waves in the Blasius boundary layer may evolve through several weakly nonlinear regimes before ending up with the same, fully nonlinear, inviscid triple-deck system. For the purpose of this paper, it is sufficient to point out

that the above scenario that provides some clues to the possible nonlinear fate of the instability modes. The detailed numerical study, which is clearly necessary to validate the particulars of this scenario, is outside the scope of the present work.

A final noteworthy feature of the overall nonlinear development is that the Klebanoff distortion exerts its influence only during stages I and II and that its effect is felt only as a higher-order correction during stage III. In other words, the Klebanoff distortion is likely to serve only as a catalyst that promotes the early growth of the disturbance, which eventually evolves into the same canonical regime of inviscid strongly nonlinear behaviour as that predicted for an unperturbed Blasius flow.

We emphasize that the results of the nonlinear theory should be treated with some caution. While the prediction that the evolution would occur over progressively shorter length scales is broadly in agreement with experimental observations, the formation of the final singularity is certainly non-physical. It is also possible that the strong nonlinearity in the fully nonlinear triple-deck stage would prevent the occurrence of the above singularity. Another effect that may alter the nonlinear behaviour is non-parallelism of the basic state, which is suppressed when integrating the nonlinear evolution equations. Even though this effect is small in the strict asymptotic sense, it may be significant for the moderate Reynolds numbers encountered in practice.

5. Spanwise-periodic distortion

Having examined the case of spanwise localized Klebanoff distortions thus far, we now briefly consider the instability characteristics in the presence of global, but spanwise-periodic distortions. Specifically, in § 5.1, we apply Floquet theory to study the instability modes first considered in § 3. In § 5.2, we examine the analogy, for a non-stationary distortion, of the Goldstein–Wundrow (1995) (G–W) modes, which are associated with a subharmonic parametric resonance. The relation between the Floquet and the G–W modes is discussed in § 5.3.

5.1. *Floquet modes*

Let us now examine how the results in §§ 3–4 need to be modified in the case of a spanwise-periodic wall-shear perturbation $\lambda_D(Z;\bar{x},t)$. As mentioned earlier, (3.25) still holds in this case, but its solution according to Floquet theory takes the form

$$\Phi = \hat{\Phi}\,\mathrm{e}^{\mathrm{i}\mu Z}, \tag{5.1}$$

where μ is a real number, with $\mu = 0$ denoting a fundamental mode and $\mu = 1$ being the subharmonic mode. The periodic function $\hat{\Phi}$ is governed by

$$\hat{\mathscr{L}}\hat{\Phi} \equiv \hat{\Phi}_{ZZ} + 2\mathrm{i}\mu\hat{\Phi}_Z - \mu^2\hat{\Phi} + \psi(Z)\hat{\Phi} = \alpha_s\hat{\Phi}, \tag{5.2}$$

where $\psi(Z)$ is related to the wall-shear fluctuation λ_D as defined in (3.26). The operator $\hat{\mathscr{L}}$ is Hermitian, so that its adjoint is simply its complex conjugate, $\hat{\mathscr{L}}^*$. It also follows that the adjoint eigensolution is correspondingly given by the complex conjugate of Φ. In view of the Hermitian property, the second-order term in the perturbation expansion (3.2)–(3.5) merely leads to a correction to the streamwise wavenumber similar to that for the localized distortion. At the fourth order, again, one finds (3.27) as obtained earlier in § 3. On writing $\Phi_2 = \hat{\Phi}_2\,\mathrm{e}^{\mathrm{i}\mu Z}$, multiplying both sides of the resultant equation, by $\hat{\Phi}^*$ and integrating the resulting equation over the spanwise wavelength L, we obtain the amplitude evolution equation $A_X = (\gamma_0 + \kappa_d)A$

where the excess growth rate κ_d is given by

$$\kappa_d = \int_0^L \gamma(Z)|\hat{\Phi}|^2 \, \mathrm{d}Z, \tag{5.3}$$

provided that Φ is normalized such that $\int_0^L |\Phi|^2 \, \mathrm{d}Z = 1$. The function $\gamma(Z)$ is related to the wall torsion of the Klebanoff distortion profile (see (3.28)).

As in Part 1, a perturbation analysis can be carried out for the limiting case of small distortion amplitudes $\psi \ll 1$, and this leads to

$$\alpha_s = -1 \pm \left(q_c^2 + 4\mu^2\beta^2\right)^{1/2}, \quad \hat{\Phi} = \left(\frac{\pi}{2\beta}\right)^{1/2} \cos\beta Z + O(\psi), \tag{5.4}$$

with

$$\beta = \pi/L, q_c = \frac{\beta}{\pi}\int_0^{\pi/\beta} \psi(Z)\cos(2\beta z) \, \mathrm{d}Z.$$

Inserting $\hat{\Phi}$ into (5.3) to calculate the excess growth rate, one finds the total growth rate

$$\kappa_r \equiv \kappa_d + \gamma_0 = \frac{2\beta}{\pi}\int_0^{\pi/\beta} \gamma(Z)\cos^2(\beta z) \, \mathrm{d}Z - \frac{\pi c_0^4}{4\lambda}. \tag{5.5}$$

As an example, the calculations will be carried out for the simple harmonic potential function

$$\psi(Z) = B_0 \cos(2\beta Z)$$

where B_0 denotes a measure of the distortion amplitude. Unlike the localized modes, Floquet modes exist for both positive and negative B_0, but it is sufficient just to consider the case of $B_0 > 0$ since

$$\alpha_s(-B_0) = \alpha_s(B_0), \quad \hat{\Phi}(Z, -B_0) = \hat{\Phi}\left(Z + \frac{\pi}{2\beta}, B_0\right). \tag{5.6}$$

The small-amplitude limit ($B_0 \to 0$) for the simple harmonic potential corresponds to

$$\alpha_s = -1 \pm \left(\tfrac{1}{4}B_0 + 4\mu^2\beta^2\right)^{1/2}, \tag{5.7}$$

which implies that two separate branches of unstable eigensolutions exist. Analytic continuation of these two branches to finite values of B_0 and μ will be referred to as branches I and II, respectively.

The relative importance of the two branches may be assessed by considering the 'unit growth rates', defined via

$$\kappa_0 = \int_0^{\pi/\beta} \cos(2\beta Z)|\Phi|^2 \, \mathrm{d}Z.$$

The variation of κ_0 with μ is shown in figure 11(*a, b*) for three values of the distortion amplitude B_0. At each of those amplitudes, the subharmonic mode ($\mu = 0$) has the largest growth rate, but the peak becomes less prominent as B_0 increases. The branch-I modes are generally more unstable than the branch-II modes. Figure 11(*b*) suggests that the unit growth of the subharmonic mode along branch II is a decreasing function of the amplitude parameter B_0.

Relations (5.6) imply that the mode for a negative B_0 corresponds to a $\pi/(2\beta)$ shift in Z of the mode for a positive B_0. Since B_0 changes its sign during each cycle of the Klebanoff fluctuation, the streak oscillation associated with the instability is expected to meander in the spanwise direction.

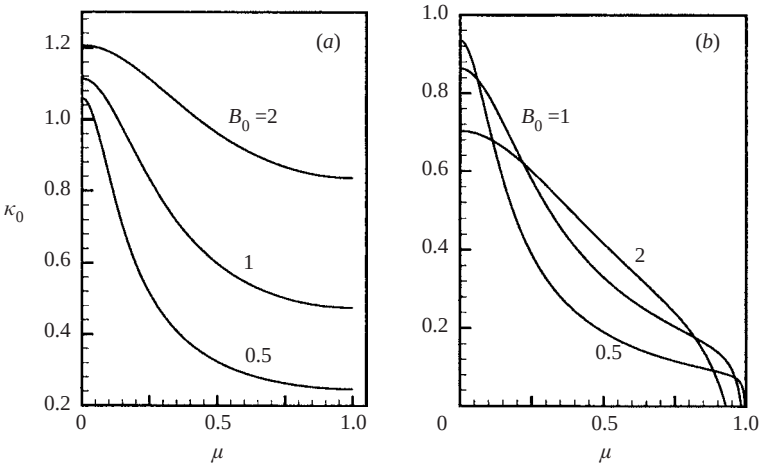

FIGURE 11. 'Unit growth rates' of Floquet modes vs. μ. (*a*) branch-I modes; (*b*) Branch-II modes. Curves correspond to $B_0 = 0.5, 1, 2$.

It can be shown that the nonlinear amplitude equations (4.2) and (4.11), which were originally derived for a localized distortion, are also valid for the case of a periodic distortion, except that the integral in the definition of Γ (see 4.3)) now is over a single wavelength in the spanwise direction.

5.2. *Goldstein–Wundrow (G–W) modes*

As alluded to in the Introduction, a periodic distortion may also be unstable to the G–W modes (Goldstein & Wundrow 1995) at distances $l^* = O(k_1^{-1}\Lambda)$ from the leading edge. Similarly to the local modes considered in §§ 3–4, the G–W modes arise because the curvature of the distortion is comparable with that of the Blasius profile in a wall layer corresponding to $\hat{y} \sim \hat{\sigma}$, such that

$$\epsilon_D \hat{\sigma} k_1^{-1} \sim \hat{\sigma}^2. \tag{5.8}$$

The G–W modes also have $O(\hat{\sigma}^{-1})$ streamwise wavelengths relative to the boundary-layer thickness $R^{-1/2}l^*$. Unlike the Floquet modes, however, both spanwise and streamwise length scales of the G–W modes are comparable with the spanwise period of the distortion. Thus

$$\frac{R^{-1/2}l^*}{\Lambda} \sim \hat{\sigma}. \tag{5.9}$$

Relations (5.8)–(5.9) imply that the threshold disturbance amplitude required for the onset of the G–W modes is given by

$$\epsilon_D \sim \left(\frac{l^* R_\Lambda}{\Lambda}\right)^{-1/2} \sim (R_\Lambda/k_1)^{-1/2}. \tag{5.10}$$

Accordingly, we write

$$\epsilon_D = (R_\Lambda/k_1)^{-1/2} B_0,$$

where $B_0 = O(1)$ denotes the scaled amplitude of the distortion. A G–W mode consists of a pair of oblique waves, and it can be expanded in the same form as the Floquet modes, i.e. the main-deck eigensolutions are given by (3.2)–(3.5), except that

$\hat{\sigma}^{3/2}$ in (3.4) is replaced by $\hat{\sigma}$, and

$$\hat{\sigma} = \left(\frac{l^*}{\Lambda R_\Lambda}\right)^{1/2}, \quad A\Phi(Z) = \mathrm{e}^{\kappa X}(\mathrm{e}^{\mathrm{i}\beta Z} \pm \mathrm{e}^{-\mathrm{i}\beta Z}). \tag{5.11}$$

The $\pm$ signs signify two separate families of instability modes. Even though modes from these two families are trivially related to each other via a shift in Z by $\pi/(2\beta)$, modes from both families must be considered, in general. Since a G–W mode involves subharmonics of the Klebanoff distortion, its amplification can be attributed to a parametric resonance mechanism.

Similarly to the local and the Floquet modes, the Klebanoff distortion in the bulk of the boundary layer leads to an $O(\hat{\sigma})$ correction to the phase speed. However, for the present periodic case, the above process is completely passive in the sense that it does not affect either the growth rate or the shape of the instability mode. The instability characteristics are solely controlled by the curvature of the distortion, exactly as in Goldstein & Wundrow (1995). Substituting the curvature of the present distortion into their equation (6.22), we obtain the total growth rate of a G–W mode induced by a Klebanoff distortion:

$$\kappa_r = \frac{2\cos\theta}{1+\cos^2\theta}\left\{\pm\frac{\pi c_0^3}{\lambda^2(2\bar{x})^{3/2}}\cos 2\theta\,\Omega_c(\bar{x},\bar{t}) - \frac{\pi c_0^4}{4\lambda} + \frac{\lambda^2}{2R^{1/4}\hat{\sigma}^5(2\alpha_0 c_0)^{1/2}}\right\}, \tag{5.12}$$

where $\theta = \tan^{-1}(\beta/\alpha_0)$, $c_0 = (\alpha_0^2+\beta^2)^{1/2}\lambda$, and

$$\Omega_c(\bar{x},\bar{t}) = -\left\{\frac{\beta}{2\pi}\int_0^{2\pi/\beta} w_s'(Z)\cos(2\beta Z)\,\mathrm{d}Z\right\}\{\bar{U}'''(0,\bar{x})\,\mathrm{e}^{-\mathrm{i}\bar{t}} + \text{c.c.}\}. \tag{5.13}$$

For the excess growth rate induced by the Klebanoff distortion to be dominant, the disturbance amplitude must satisfy $\hat{\sigma} \gg R^{-1/20}$. Additionally, we must have $\hat{\sigma} \ll 1$ in order for the foregoing analysis to be valid. The above two considerations imply that the result (5.12) is valid if the wavelength of the Klebanoff fluctuation is in the range

$$R_\Lambda^{9/11} \ll \frac{l^*}{\Lambda} \ll R_\Lambda, \tag{5.14}$$

or, alternatively, if the amplitude of the free-stream disturbance lies within

$$R_\Lambda^{-1} \ll \epsilon_D \leqslant R_\Lambda^{-10/11}. \tag{5.15}$$

The result (5.12) indicates that omission of one of the modes, for example the minus mode, will lead to the erroneous conclusion that a distortion with positive $\Omega_c > 0$ will not be able to support (inviscid) instability waves with $\cos 2\theta < 0$. Again, for a Klebanoff distortion, Ω_c changes its sign during the modulation cycle and, therefore, there must be a switching between the plus and minus modes during this cycle.

Calculations were performed for $w_s'(Z) = B_0\cos(2\beta Z)$ and selected values of β. In figure 12, we show the inviscid growth rate (i.e. κ_r with the last term in (5.12) dropped), as a function of the wavenumber α_0. For small and moderate values of β, the peak growth rate occurs near $\alpha_0 = 0.45$. The peak growth rate decreases and is eventually stabilized, as β is increased. For larger values of β, the dominant instability modes emerge at small α values, centred at $\alpha_0 \approx 0.12$.

Finally, we note that once the amplitude of the instability modes reaches the threshold range of

$$\epsilon = O(\hat{\sigma}^{10}) = O\left(\left(\frac{\Lambda R_\Lambda}{l^*}\right)^{-5}\right),$$

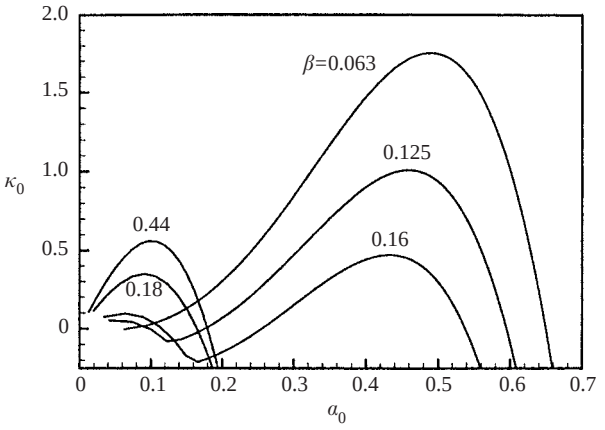

FIGURE 12. Growth rates of Goldstein–Wundrow modes. The parameters $B_0 = 4$, $\bar{x} = 1.2$ and $\bar{t} \approx -1.498$. Curves correspond to $\beta = 0.063,\ 0.125,\ 0.16,\ 0.18,\ 0.44$.

the function $A(X, Z)$ must be written as

$$A = \tilde{A}(X)(\mathrm{e}^{\mathrm{i}\beta Z} \pm \mathrm{e}^{-\mathrm{i}\beta Z}),$$

where the amplitude function $\tilde{A}$ is governed by the nonlinear equation derived previously by Goldstein & Choi (1989) and Wu, Lee & Cowley (1993).

5.3. *The relation between Floquet modes and G–W modes*

The G–W modes and Floquet modes considered in § 5.1 can exist only when the Klebanoff distortion is periodic in the spanwise direction. Let us discuss the relation between them from two separate viewpoints. First, consider the stability properties at a fixed location $\bar{x} = O(1)$, and examine which type of modes emerges and how their character changes as the amplitude parameter ϵ_D is gradually increased from zero. As indicated by (2.22) and (5.10), G–W modes require a smaller threshold for the distortion amplitude than the Floquet modes, and hence the G–W modes appear first as ϵ_D is increased. That is, for ϵ_D specified by (5.10), the G–W modes correspond to the only inviscid instability that the disturbed flow can support. As ϵ_D is further increased, the streamwise wavenumber and growth rate of G–W modes (which are $O(\epsilon_D k_1^{-1})$ and $O((\epsilon_D k_1^{-1})^4)$, respectively) increase as well. Because the spanwise wavenumber must remain fixed, the G–W modes become progressively 'two-dimensional'. To investigate this large-amplitude limit (namely $B_0 \gg 1$ or $\epsilon_D \gg (R_\Lambda/k_1)^{-1/2}$), we introduce the rescaled wavenumber and phase speed via

$$(\alpha_0, c_0) = B_0(\tilde{\alpha}_0, \tilde{c}_0).$$

Inserting these into (5.12) and taking the limit $B_0 \to \infty$ reduces (5.12) to

$$\kappa_r = B_0^4 \left\{ \pm \frac{\pi \tilde{c}_0^3}{\lambda^2 (2\bar{x})^{3/2}} \Omega_c(\bar{x}, \bar{t}) - \frac{\pi \tilde{c}_0^4}{4\lambda} \right\}, \tag{5.16}$$

which corresponds to the small-distortion-amplitude limit of the growth rate of Floquet modes. More precisely, the large-amplitude behaviour (5.16) remains valid until $B_0 = O((k_1 R_\Lambda)^{1/6})$, i.e. $\epsilon_D \sim O(R_\Lambda^{-1/3} k_1^{2/3})$, which corresponds to the threshold magnitude of the distortion for the Floquet modes to arise (see (2.22)). At this stage, the enhanced streamwise growth of the instability modes is balanced by the spanwise modulation in the main part of the boundary layer. Thus, we have shown that the

G–W and Floquet modes exist in separate regimes of distortion amplitude, and that the large-distortion limit of the G–W modes 'matches' to the small-distortion limit of the Floquet modes.

An alternative way to view the relation between G–W and Floquet modes is to consider the instability characteristics for a fixed distortion strength ϵ_D, and examine how these modes emerge and evolve as the streamwise location is varied. Suppose that $\epsilon_D \sim O(R_A^{-1/3} k_1^{2/3})$ as specified by (2.22), so that the distorted flow supports Floquet modes at $\bar{x} = O(1)$. Given that the threshold distortion strength for G–W modes is much smaller, one may expect them to exist in the upstream region $\bar{x} \ll 1$. The link between the upstream G–W modes and Floquet modes is best revealed by examining the small-$\bar{x}$ asymptote of the Floquet modes. If one takes into account the streamwise variation of the distortion as well as of the Blasius flow, the key balance (2.19) can be expressed more precisely as

$$\epsilon_D k_1^{-1} \bar{U}_{D,YYY}(0, \bar{x}) Y_c \sim \hat{\sigma} \lambda^2 Y_c^2, \tag{5.17}$$

where $Y_c = c_0/\lambda = \alpha_0/\lambda^2$ is the scaled critical level. Since $\bar{U}_{D,YYY} \sim (\bar{x})^{-3/2} U'''$, and $\bar{U}'''(0, \bar{x}) \to (-\mathrm{i}\lambda_0 \bar{x}^2)$ (as indicated by (2.15) and (2.16)), relation (5.17) shows that $Y_c \sim \bar{x}^{3/2}$ and hence $\alpha_0 \sim \bar{x}^{1/2}$, $c_0 \sim \bar{x}$, as $\bar{x} \to 0$. This suggests the rescaling

$$(\alpha_0, c_0) = \left(\bar{x}^{1/2} \tilde{\alpha}_0, \bar{x}\, \tilde{c}_0\right). \tag{5.18}$$

In the limit $\bar{x} \to 0$, the potential ψ in (5.2) becomes vanishingly small, and so the result (5.5) applies. Substituting (5.18) into (5.5), and using (3.26) and the fact that $\bar{U}'''(0, \bar{x}) \to -\mathrm{i}\lambda_0 \bar{x}^2$, we find

$$\kappa_r = \bar{x}^{9/2} \left\{ \frac{\pi \tilde{c}_0^3}{\lambda_0^2 2^{3/2}} \tilde{\Omega}_c - \frac{\pi \tilde{c}_0^4}{4\lambda_0} \right\}, \tag{5.19}$$

where $\lambda_0 = 0.33206$, and

$$\tilde{\Omega}_c \equiv -\left\{ \frac{\beta}{\pi} \int_0^{\pi/\beta} w_s'(Z) \cos(2\beta Z)\, \mathrm{d}Z \right\} (-\mathrm{i}\lambda_0\, \mathrm{e}^{-\mathrm{i}\bar{t}} + \text{c.c.}).$$

The above approximation becomes invalid when $\bar{x} = O(k_1 R_A)^{-1/3}$, at which stage the streamwise wavenumber becomes comparable with the spanwise wavenumber so that the modes become fully three-dimensional in character. Thus, the G–W modes operate in the region where $\tilde{x} \equiv (k_1 R_A)^{1/3} \bar{x} = O(1)$, and their growth rates are given by (5.12), provided $\bar{x}$ is replaced by $\tilde{x}$, and $\bar{U}'''$ in (5.13) by its upstream asymptote $(-\mathrm{i}\tilde{x}^2 \lambda_0)$. Clearly, the large-$\tilde{x}$ limit of this result matches to (5.19). Thus the upstream limit of Floquet modes matches to the downstream limit of the G–W modes, i.e. the Floquet modes represent the downstream continuation of the G–W modes.

Note that the above matching between the G–W and the Floquet modes was based on the assumption of linear instability, at least through the region of overlap between the two. In reality, of course, the upstream G–W modes might reach a nonlinear stage of evolution first and, hence, bypass the evolution into Floquet modes.

6. Conclusions and discussion

In this paper, we have investigated the effect of long-wavelength Klebanoff fluctuations on the instability of a Blasius boundary layer. By using an asymptotic approach based on the high-Reynolds-number assumption, we derived a consistent, albeit simplified, mathematical model, which appears to capture certain key elements of this problem. Specifically, our analysis indicates that relatively weak Klebanoff

fluctuations, which do not alter the velocity profile by $O(1)$, may change the near-wall curvature of the underlying Blasius flow by $O(1)$. This, in turn, has the effect of modifying and even fundamentally altering the instability characteristics of the boundary-layer flow. Specifically, the perturbed flow can support primarily two-dimensional instability modes that may be localized in the spanwise direction. The spanwise distribution of these modes is controlled by the distortion via a Schrödinger equation governing the mode shape, in which the local skin friction of the Klebanoff distortion acts as a potential. The growth rates of these modes are determined by the wall torsion of the perturbed flow.

When the distortion is just strong enough to produce an excess growth comparable with viscous growth, the above-mentioned instability modes may be viewed as modified T–S waves. However, as the strength of the distortion exceeds a threshold range (in an asymptotic sense), the instability becomes essentially inviscid, and the characteristic frequencies and growth rates are now much higher than those of the T–S waves in an unmodified Blasius flow. A localized distortion (such as may be induced when the spanwise correlation length of the free-stream disturbance is small) may induce both sinuous and varicose modes of instability. However, the sinuous modes are found to be more unstable, in general. Because the Klebanoff distortion modulates the base flow in both $\bar{t}$ and $\bar{x}$, its effect on the instability is intermittent in time and localized in space, i.e. it is manifested only during a certain phase of the modulation and in a limited window along the streamwise direction. For a localized Klebanoff distortion, for instance, the dominant sinuous modes appear only during that phase in which the distortion is characterized by a dominant low-speed streak. A spanwise-periodic distortion is found to support analogous but spatially quasi-periodic modes through parametric resonance. Even though we assumed the Klebanoff distortion to have a single frequency for the most part, the theory itself is quite general, being equally relevant to a wider spectrum of vortical free-stream disturbances.

An interesting feature of the instability modes identified in this paper is that, despite the low-frequency nature of the Klebanoff distortion, the unsteadiness of the distortion plays a crucial role in this model. (Leib *et al.* 1999 had shown earlier that it is also important to account for this unsteadiness for correctly predicting the Klebanoff distortion itself.) Specifically, the above instability modes would not have been present for a small-amplitude Klebanoff distortion if it was treated as being steady. Moreover, the intermittent nature and the convection of unstable patches are both attributed to the unsteadiness of the distortion.

The nonlinear development of a localized sinuous instability mode was also studied. In stage I of this evolution, the mode amplitude is governed by an integro-ordinary-differential equation, the solution of which develops a finite-distance singularity if the viscous effect is not too large, but decays if the viscosity parameter exceeds a critical value. In the vicinity of the singularity, the disturbance enters the second regime, in which its evolution takes place over a much shorter scale and is governed by integro-partial-differential equation. While in the first stage the spanwise modal shape remains unaffected by nonlinearity; in the second regime, it undergoes nonlinear deformation due to the simultaneous modulation by the distortion and nonlinear effects. The solution appears to develop yet another singularity during nonlinear stage II, which completes the metamorphosis of the initially linear instability into fully nonlinear inviscid disturbances that are generic to the strongly nonlinear phase of disturbance evolution. It appears reasonable to suggest that the temporarily intermittent and spatially localized instability and its subsequent nonlinear development lead to patches of streak oscillations.

The qualitative predictions of our theory are consistent with laboratory observations. Our results indicate that the streaks can become unstable even without appreciable changes in the Blasius profile. This is precisely what Matsubara *et al.* (2000) concluded on the basis of their experimental studies. (See, also, Matsubara & Alfredsson 2001.) The predicted patches of oscillations have been observed in their experiments. The elevated growth of instability wavepackets in the presence of Klebanoff distortion has also been observed in the experiments by Kendall (1991).

The seemingly puzzling and conflicting experimental observations can be reconciled to some degree when reinterpreted in the light of our theoretical results. As mentioned in § 1, the wavepackets develop out of the background disturbance and amplify downstream. Kendall (1990) associated these with T–S waves. We believe that they are likely to be packets of the local T–S waves identified in this paper rather than the usual T–S waves in an unmodified Blasius flow. These local T–S waves exhibit virtually all of the unusual characteristics observed by Kendall: the onset threshold, the excess growth, and the range of higher frequencies. Since their growth rates depend on the magnitude of the Klebanoff fluctuation, it is to be expected that their amplitude at a particular observation point should have a nonlinear relation to the magnitude of the Klebanoff motion. Since the spanwise extent of these local T–S modes is determined by the Klebanoff distortion, it is not surprising that their lateral spreading rate is much smaller than that of a usual T–S wavepacket. What remains unknown is the receptivity mechanism for the packets of these local T–S waves.

The extreme sensitivity of the boundary-layer response to harmonic point excitation (Watmuff 1997, 1998) could also be explained in the light of the present work. In the presence of Klebanoff fluctuations, a point excitation definitely generates local T–S modes as well. Therefore, the general response cannot be represented as a summation of the conventional T–S waves only, as was assumed in the calculation. This may be the reason why a meaningful comparison was impossible unless the Klebanoff fluctuation is substantially reduced.

The effect of Klebanoff distortions on a planar T–S wave appears to be rather controversial (cf. Boiko *et al.* 1994; Watmuff 2000). In this work, we did not explore this phenomenon in detail. However, one might expect that the continuous spectrum of (3.25) might be involved in explaining the observed deformation (i.e. scattering) of the wave front by the Klebanoff fluctuation. This could be a topic for future investigation. It might also be useful to examine the connection between the instability modes examined herein and pure T–S waves, i.e. whether (and to what degree) the above modes actually emerge from existing T–S waves at appropriate locations (and/or instants) during the modulation cycle and eventually degenerate into them at the end of the transient window of instability (if they cannot reach nonlinear amplitudes by then). Such issues can be exceedingly subtle, as demonstrated by P. Hall (2001, personal communication) for the case of a (spatially homogeneous) unsteady Stokes layer.

Jacobs & Durbin (2001), based on their direct numerical simulations of bypass transition, concluded that the streaks close to the wall are stable. Only when the streaks lift up to the edge of the boundary layer to form a 'backward jet' do they break down into turbulent spots. Our results seem to be in conflict with this finding. There could be a number of reasons for the disagreement. It might be that the present instability is too weak and that it is masked by other more vigorous processes. Alternatively, it is plausible that the instability modes identified herein were not excited in their simulations. Finally, unlike experimental spectra which tend to be dominated by low-frequency components (see e.g. figure 13 of Kendall 1998), the energy of the free-stream

disturbances in their simulation is contained in a band of rather high frequencies (an order-of-magnitude higher than typical frequencies of T–S waves) and, therefore, the streaks are not a linear response to the low-frequency components. Rather, they are generated nonlinearly by the interaction of higher-frequency components. The question as to whether this is the cause of the discrepancy remains open at this point.

In the present work, the instability modes are identified by effectively freezing the background velocity profile, and hence represent the instantaneous behaviour of the instability. This is justified on the basis of the disparity of time scales between the low-frequency Klebanoff distortions and the high-frequency instability modes. On the other hand, since the distorted flow is time periodic, it may support global Floquet modes. There arises a question as to how the instantaneous instability is related to the global mode of Floquet type, i.e. how a given disturbance entity evolves through multiple modulation cycles in time and/or in space. In the linear context, i.e. assuming that the nonlinear effects do not come into play within a single modulation cycle (in time and space) subsequent to the genesis of the instability mode, it may be possible to pursue a multi-dimensional Floquet theory (i.e. Floquet analysis in both $\bar{x}$ and $\bar{t}$) within a finite-Reynolds-number framework in order to examine how the local/instantaneous modes are linked to the global Floquet ones. Such a line of attack has recently been taken by P. Hall (2001, personal communication) on the analogous problem for time-periodic (but spatially homogeneous) Stokes layer. Hall finds that the phase speeds of certain instantaneously growing modes, if continued into their decaying phase, have a periodic dependence on time, and thus these modes correspond to the high-Reynolds-number version of the Floquet modes. However, all such modes are found to be globally stable, which suggests that local modes rather than the global modes are the cause of transition, at least in the Stokes-layer case. The issue of local versus Floquet modes becomes more complicated for the doubly inhomogeneous basic state examined herein. Given that the existence of global Floquet modes relies on the periodicity of the distortion, while the Klebanoff distortion in reality is random, it seems reasonable to speculate that the instantaneous modes examined herein would be more relevant in practice, and that such modes could grow sufficiently within a single 'window' of instability to induce strongly nonlinear behaviour.

The present work is, of course, far from being a complete or quantitatively accurate description of the problem. Nonetheless, the simplicity of the current model, together with the physical insights derived from it, appear to justify the assumptions made herein. The theory, we believe, sheds useful light on a very complex process which has so far eluded a first-principles explanation. The primary shortcoming of the present theory corresponds to its neglect of the spanwise ellipticity of the Klebanoff fluctuation. The theory of course does not apply when the free-stream disturbance is sufficiently strong that the distortion becomes fully nonlinear. The more general problem for Klebanoff distortions with an $O(1)$ wavelength, including the effects of nonlinearity and stochasticity, is currently under investigation. Because no analytical techniques currently exist to deal with stochastic eigenvalue problems with $O(1)$ stochastic parameters, we are pursuing a Monte Carlo approach in an attempt to quantify the expected growth rate of the instability modes for a given r.m.s. amplitude (and wavenumber/frequency spectrum) of the free-stream disturbance.

The work of X.W. was carried out during his sabbatical in 2001 at ICASE, NASA Langley and the Center for Turbulence Research, Stanford University (USA). He would like to acknowledge the hospitality and financial support of these institutions. It is a great pleasure to thank Professors Parviz Moin, Paul Durbin, W. C. Reynolds

and Peter Bradshaw for helpful discussions and comments pertaining to this work. We also acknowledge input from the reviewers which has led to an improved presentation of the results.

REFERENCES

Andersson, P., Brandt, L., Bottaro, A. & Henningson, D.-S. 2001 On breakdown of boundary layer streaks. *J. Fluid Mech.* **428**, 29–60.

Arnal, D. & Juillen, J. C. 1978 Contribution experimental a l'etude de la receptivite d'une couche limite laminaire, a la turbulence de l'ecoulement general. *ONERA Tech.* 1/5018 AYD.

Bakchinov, A. A., Westin, K. J. A, Kozlov, V. V. & Alfredsson, P. H. 1998 Experiments on a localized disturbances in a flat plate boundary layer. Part 2. Interaction between localized disturbances and TS-waves. *Eur. J. Mech.* B/*Fluids* **17**, 847–873.

Boiko, A. V., Westin, K. J. A., Klingmann, B. G. B., Kozlov, V. V. & Alfredsson, P. H. 1994 Experiments in a boundary layer subjected to free stream turbulence. Part 2. The role of TS-waves in the transition process. *J. Fluid Mech.* **281**, 219–245.

Bradshaw, P. 1965 The effect of wind-tunnel screens on nominally two-dimensional boundary layers. *J. Fluid Mech.* **22**, 679–687.

Choudhari, M. 1996 Boundary-layer receptivity to three-dimensional unsteady vortical disturbances in free stream. *AIAA Paper* 96-0181.

Cowley, S. J. & Wu, X. 1994 Asymptotic methods and solutions in transition modeling. *Progress in Transition Modelling, AGARD Rep.* 793.

Crow, S. C. 1966 The spanwise perturbation of two-dimensional boundary layers. *J. Fluid Mech.* **24**, 153–164.

Dryden, H. L. 1936 Air flow in the boundary layer near a plate. *NACA Rep.* 562.

Gaster, M. 1962 A note on the relation between temporally-increasing and spatially-increasing disturbances in hydrodynamic stability. *J. Fluid Mech.* **14**, 222–224.

Goldstein, M. E. 1994 Nonlinear interactions between oblique instability waves on nearly parallel shear flows. *Phys. Fluids* A **6**, 724–735.

Goldstein, M. E. & Choi, S.-W. 1989 Nonlinear evolution of interacting oblique waves on two-dimensional shear layers. *J. Fluid Mech.* **207**, 97–120, and Corrigendum **216**, 1990, 659–663.

Goldstein, M. E. & Durbin, P. A. 1986 Nonlinear critical layers eliminate the upper branch of spatially growing Tollmien–Schlichting waves. *Phys. Fluids* **29**, 2334–2345.

Goldstein, M. E. & Leib, S. J. 1993 Three-dimensional boundary-layer instability and separation induced by small-amplitude streamwise vortices in the upstream. *J. Fluid Mech.* **246**, 21–41.

Goldstein, M. E. & Wundrow, D. W. 1995 Interaction of oblique instability waves with weak streamwise vortices. *J. Fluid Mech.* **284**, 377–407.

Goldstein, M. E. & Wundrow, D. W. 1998 On the environmental realizability of algebraically growing disturbances and their relation to Klebanoff modes. *Theor. Comput. Fluid Dyn.* **10**, 171–186.

Gulyaev, A. N., Kozlov, V. E., Kuznetson, V. R., Mineev, B. I. & Sekundov, A. N. 1989 Interaction of laminar boundary layer with external turbulence. *Izv. Akad. Nauk SSSR Mekh. Zhid. Gaza.* **6**, 700–710.

Haberman, R. 1972 Critical layers in parallel shear flows. *Stud. Appl. Maths* **50**, 139.

Jacobs, R. G. & Durbin, P. A. 2001 Simulations of bypass transition. *J. Fluid Mech.* **428**, 185–212.

Kendall, J. M. 1985 Experimental study of disturbances produced in pre-transitional laminar boundary layer by weak free stream turbulence. *AIAA Paper* 85-1695.

Kendall, J. M. 1990 Boundary-layer receptivity to free-stream turbulence. *AIAA Paper* 80-1504.

Kendall, J. M. 1991 Studies on laminar boundary layer receptivity to freestream turbulence near a leading-edge. In *Boundary Layer Stability and Transition to Turbulence* (ed. D. C. Reda, R. H. Reed & R. Kobayashi). ASME FED, vol. 114, pp. 23–30.

Kendall, J. M. 1998 Experiments on boundary-layer receptivity to freestream turbulence. *AIAA Paper* 98-0530.

Klebanoff, P. S. 1971 Effect of free-stream turbulence on a laminar boundary layer. *Bull. Am. Phys. Soc.* **10**, 1323.

Leib, S. J., Wundrow, D. W. & Goldstein, M. E. 1999 Effect of free-stream turbulence and other vortical disturbances on a laminar boundary layer. *J. Fluid Mech.* **380**, 169–203.

Matsubara, M. & Alfredsson, P. H. 2001 Disturbance growth in boundary layers subjected to free-stream turbulence. *J. Fluid Mech.* **430**, 149–168.

Matsubara, M., Bakchinov, A. & Alfredsson, P. H. 2000 Growth and breakdown of streaky structures in boundary layer transition induced by free stream turbulence. In *Proc. IUTAM Symp. on Laminar-Turbulent Transition* (ed. H. Fasel & W. Saric), pp. 371–376. Springer.

Rai, M. M. & Moin, P. 1993 Direct numerical simulation of transition and turbulence in a spatially evolving boundary layer. *J. Comput. Phys.* **109**, 169–192.

Schlichting, H. 1933 Zur entstehung der turbulenz bei der plattenstromung. *Nachr. Ges. Wiss. Göttingen Math.-Phys.*, 181–208.

Schubauer, G. B. & Skramstad, H. K. 1947 Laminar boundary-layer oscillations and transition on a flat plate. *J. Res. Nat. Bur. Stand.* **38**, 251–292.

Smith, F. T. 1979 On the nonparallel flow stability of the Blasius boundary layer. *Proc. R. Soc. Lond.* A **366**, 91–109.

Taylor, G. I. 1939 Some recent developments in the study of turbulence. *Proc. 5th Intl Congress for Applied Mechanics* (ed. J. P. Den Hartog & H. Peters), pp. 294–310. Wiley.

Timoshin, S. N. & Smith, F. T. 1997 Singular modes in Rayleigh instability of three-dimensional streamwise-vortex flows. *J. Fluid Mech.* **333**, 139–160.

Tollmien, W. 1929 Über die Entstehung der Turbulenz. *Nachr. Ges. Wiss. Göttingen Math.-Phys.*, 21–44.

Watmuff, J. H. 1997 Interactions between Klebanoff modes and TS waves in a Blasius boundary layer. *AIAA Paper* 97-0558.

Watmuff, J. H. 1998 Detrimental effects of almost immeasurably small freestream nonuniformities generated by wind-tunnel screens. *AIAA J.* **36**, 379–386.

Watmuff, J. H. 2000 Distortion of Tollmien–Schlichting waves by leading-edge vortices. *Proc. IUTAM Symp. on Laminar-Turbulent Transition* (ed. H. Fasel & W. Saric), pp. 333–338. Springer.

Westin, K. J., Boiko, A. V., Klingmann, B. G. B., Kozlov, V. V. & Alfredsson, P. H. 1994 Experiments in a boundary layer subjected to free stream turbulence. Part 1. Boundary layer structure and receptivity. *J. Fluid Mech.* **281**, 193–218.

Wu, X. 1993 Nonlinear temporal-spatial modulation of near-planar Rayleigh waves in shear flows: formation of streamwise vortices. *J. Fluid Mech.* **256**, 685–719.

Wu, X., Lee, S. S. & Cowley, S. J. 1993 On the weakly nonlinear three-dimensional instability of shear flows to pairs of oblique waves: the Stokes layer as a paradigm. *J. Fluid Mech.* **253**, 681–721.

Wu, X. & Luo, J. 2003 Linear and nonlinear instabilities of a Blasius boundary layer perturbed by streamwise vortices. Part 1. Steady streaks. *J. Fluid Mech.* **483**, 225–248.

Wu, X., Stewart, P. A. & Cowley, S. J. 1996 On the weakly nonlinear development of Tollmien–Schlichting wave-trains in boundary layers. *J. Fluid Mech.* **316**, 133–171.

Wu, X., Leib, S. J. & Goldstein, M. E. 1997 On the nonlinear evolution of a pair of oblique Tollmien–Schlichting waves in boundary layers. *J. Fluid Mech.* **340**, 361–394.

Wundrow, D. W. & Goldstein, M. E. 2001 Effect on a laminar boundary layer of small-amplitude streamwise vorticity in the upstream flow. *J. Fluid Mech.* **426**, 229–262.